Trade-off between light deprivation and desiccation in intertidal seagrasses due to periodic tidal inundation and exposure: insights from a data-calibrated model

Xinyan Wang[1,2,3], Matthew P. Adams[2,4,5], Dongdong Shao[1,3*]

[1]State Key Laboratory of Water Environment Simulation & School of Environment, Beijing Normal University, Beijing 100875, China.

[2]School of Mathematical Sciences, Queensland University of Technology, Brisbane, QLD 4000, Australia.

[3]Yellow River Estuary Wetland Ecosystem Observation and Research Station, Ministry of Education, Dongying, Shandong 257000, China.

[4]Centre for Data Science, Queensland University of Technology, Brisbane, QLD 4000, Australia.

[5]School of Chemical Engineering, The University of Queensland, St Lucia, QLD 4072, Australia.

Corresponding author: Dongdong Shao (ddshao@bnu.edu.cn)

Key Points:

- We developed an intertidal seagrass growth model by incorporating the physiological responses to periodic tidal inundation and exposure
- Neglecting air-exposure responses substantially overestimates intertidal seagrass growth rates
- A trade-off between light deprivation and desiccation on intertidal seagrass exists, which yields an "optimal" growth elevation

Abstract

Some seagrass species thrive in shallow intertidal zones globally, adapting to periodic tidal inundation and exposure with distinctive physiological traits and offering crucial ecosystem services. However, predicting the responses of intertidal seagrasses to external stressors is hampered by the complexity of the dynamic and harsh environments they occupy. Consequently, intertidal seagrass growth models, especially those incorporating dynamic physiological responses, are scarce in the literature. Our study comprehensively collated relevant data from the literature to parameterize the relationship between air exposure, seagrass leaf water content and photosynthetic efficiency to inform new growth rate functions for generalisable intertidal seagrass growth models. We tested the applicability of these model formulations for scenarios with varying physiological process assumptions, seagrass species, tidal conditions, meadow elevations and water turbidity. We found that neglecting air-exposed physiological responses (i.e., leaf water content loss and reduced photosynthetic efficiency) can substantially overestimate seagrass growth rates. We also observed a trade-off between light deprivation and desiccation on intertidal seagrass growth under specific tidal ranges and turbidity conditions. This can yield an "optimal" elevation where overall stress of desiccation (increasing with meadow elevation) and light deprivation (decreasing with meadow elevation) are minimized. The predicted optimal elevation, i.e., the most suitable habitat for intertidal seagrass, moves upward as water turbidity increases. Our study provides conceptual and quantitative guidance for ecological modellers to include air exposure responses of intertidal seagrasses in coastal ecosystem models. The model also helps to evaluate the viability of intertidal seagrass habitats and inform decisions on coastal ecosystem management under changing environmental conditions.

Keywords: Intertidal seagrasses; Air exposure; Physiological responses; Tidal cycle; Habitat suitability

Plain Language Summary

Some seagrasses grow in intertidal zones where they are periodically exposed or submerged due to the rise and fall of tides. However, predicting how these valuable ecosystems respond to such stresses in a highly dynamic and harsh environment is difficult. Our study collated relevant data

from the literature to quantify the physiological responses of intertidal seagrasses to air exposure, and further developed intertidal seagrass growth models by incorporating these responses. We tested these models for different seagrass species and under various field conditions, and found a substantial decline in seagrass growth rates when considering air-exposure responses. We also observed that intertidal seagrass growth was affected by both light reduction (increasing with seagrass meadow elevation) and desiccation stress (decreasing with meadow elevation), and the most suitable habitat for seagrass growth is located at the elevation where the combined stress are minimal. The most suitable elevation for intertidal seagrass increases as water turbidity increases. Our model can help assess the suitability of intertidal seagrass habitats and inform decisions on coastal ecosystem management under changing environmental conditions.

1 Introduction

Seagrass meadows are among the most productive marine ecosystems in the world, and are widely distributed in both tropical and temperate coastal waters (Orth et al., 2020). Seagrasses are usually restricted by the upper depth limit due to air exposure at low tides and desiccation (Shafer et al., 2007; Suykerbuyk et al., 2018). As such, many seagrass species are intolerant to these conditions and are unable to grow in intertidal zones (Koch, 2001). However, there are some species, including a few temperate species such as *Nanozostera japonica* (*Zostera japonica*), *Z. marina*, *Z. noltei* (*Z. noltii*), as well as subtropical or tropical species such as *Halophila ovalis* and *Thalassia hemprichii*, that thrive in the shallow intertidal zones of estuaries, lagoons and other coastal areas (Colomer & Serra, 2021; Shafer et al., 2007). Intertidal seagrass meadows function as essential foraging habitats (Espadero et al., 2020) and blue carbon stock, yielding higher organic carbon burial rates than subtidal seagrasses (de los Santos et al., 2022). In recent years, seagrass meadows have experienced continuous degradation caused by multiple stressors (Waycott et al., 2009). Meanwhile, intertidal seagrass ecosystems are subject to more dynamic and harsh environments, highlighting the complexity of assessing and predicting their dynamics and interactions with environmental stressors when aiming to inform their protection and restoration.

The clear dependence of seagrass growth on environmental conditions enables the development of mathematical models to represent the physiological relationships between environmental

conditions and seagrasses (Scalpone et al., 2020). Mathematical models serve as useful tools for testing different environmental scenarios, offering insights that might not be achievable through traditional experiments. Existing seagrass models commonly include underwater light and temperature as driving forces on plant-scale processes including respiration, photosynthesis, and mortality (Elkalay et al., 2003; Piercy et al., 2023). Some models also include interspecific relationships such as the effects of algae and phytoplankton on light attenuation (Baird et al., 2016) and consumer-grazing effects (Turschwell et al., 2022). Other models expand their functionality by coupling with hydrodynamic and/or biogeochemical models to account for ecosystem-scale seagrass growth dynamics (Carr et al., 2012; Scalpone et al., 2020). However, the majority of the existing models lack the ability to simulate intertidal seagrass dynamics that are subject to periodic tidal inundation and air exposure (Erftemeijer et al., 2023; Folmer et al., 2012). To our best knowledge, only one previous study has developed formulations for the response of relative water content of intertidal seagrass leaves to different tidal conditions (Azevedo et al., 2017). However, it did not mathematically link the loss of relative water content to the photosynthetic process and subsequent vegetation growth dynamics. In the present work, we address this literature gap for the modeling of intertidal seagrasses.

Light deprivation due to tidal inundation is regarded as the most critical stressor influencing photosynthesis, growth and depth distribution of seagrasses including intertidal species (Bertelli & Unsworth, 2018; Koch, 2001). Alternatively, when exposed to air, intertidal seagrasses may exhibit photo-inhibition at high solar irradiances, and experience desiccation due to reduced leaf water content, both leading to declines in net photosynthesis (Kim et al., 2016). In addition, intertidal seagrasses may suffer from high temperatures when air-exposed, and the predominant impact of increased temperature during low tides is accelerated desiccation of seagrasses (Che et al., 2022). Conversely, many field studies have also found that intertidal seagrasses can avoid photo-inhibition due to their high tolerance to light stress without damage to photosynthetic apparatus (Clavier et al., 2011; Petrou et al., 2013). Consequently, intertidal seagrasses may take advantage of high irradiance during low tides which serve as a “window” of photosynthetic relief (Petrou et al., 2013). For example, a previous study has found that air-exposed *Z. noltei* (*Z. noltii*) in the south coast of Portugal exhibited increased productivity attributed to sustained leaf hydration (Silva et al., 2005). Yet, the same intertidal species *Z. noltei* (*Z. noltii*) in southern

Spain showed a reduced photosynthesis rate attributed to severe desiccation during air exposure (Pérez-Lloréns et al., 1994). The contrasting results suggest that desiccation, which here refers to the reduction in the leaf water content, might be the key factor determining the photosynthetic responses of intertidal seagrasses. Therefore, light deprivation and desiccation are two dominant factors controlling intertidal seagrass growth. Light deprivation can only become potentially significant in the lower intertidal zone, whereas desiccation tends to have greater importance in the intermediate and upper zones (Cabaço et al., 2009). Since light deprivation effects on seagrasses have already been captured in the vast majority of seagrass models, we propose that physiological responses of intertidal seagrasses to air exposure, especially that triggered by alteration in leaf water content, should also be included in models of intertidal seagrass growth, to more accurately simulate their growth dynamics throughout tidal cycles.

New model formulations should ideally be informed by experimental data, and several experimental studies have examined the photosynthetic responses of intertidal seagrasses to air-exposed desiccation (Jiang et al., 2014; Leuschner et al., 1998; Shafer et al., 2007). Effective quantum yield of seagrass leaves is commonly measured as a metric of photosynthetic efficiency in these studies. Thus, the relative effect of air exposure on intertidal seagrass growth dynamics can be derived from the observed relationship between effective quantum yield and relative water content for different seagrass species.

Hence, the main objectives of this study are four-fold: 1) to comprehensively collate data from experimental studies to parameterize the relationship between air exposure, relative water content of seagrass leaves and photosynthetic efficiency; 2) to develop a generalisable intertidal seagrass growth model based on these relationships throughout the tidal cycles; 3) to provide illustrative parameterisations of this model for various physiological process assumptions, tidal conditions, meadow elevation, water column turbidity, and seagrass species; and 4) to examine how model predictions of seagrass growth rates are altered by the explicit inclusion of intertidal processes. Our study provides conceptual and quantitative guidance for ecological modellers who wish to include air exposure responses of intertidal seagrasses in their coastal ecosystem models. Ultimately, it is hoped that the improved modeling made possible from this work will assist in the evaluation of viable seagrass habitats for restoration activities.

2 Methods

2.1 Context for the intertidal seagrass model

We start by describing the mathematical modeling context to articulate the scientific gap that our intertidal seagrass model fills. As is typical in seagrass growth models, we assume that carbon accumulation is the rate-limiting step for plant growth (Moreno-Marín et al., 2018; Poorter et al., 2013). The net growth *dS/dt* of seagrasses is therefore assumed to be limited by the balance between carbon gain (photosynthesis, *P*) and carbon losses (e.g., respiration *R*, mortality *m* and dissolved organic carbon exudation *E*),

$$\frac{dS}{dt} = K(P\, f_S(S) - R - E)S - mS, \quad (1)$$

where *S* represents the local quantity of seagrass (typically written in units of dry-weight biomass per ground area, g DW m^{-2}, or shoot density, shoots m^{-2}), *t* is time (d), *K* is a conversion factor that accounts for the conversion of carbon gain/loss to seagrass gain/loss (in units of g DWg^{-1} C or shoot g^{-1} C), *P* is the gross photosynthesis rate (g C g^{-1} DW d^{-1} or g C $shoot^{-1}$ d^{-1}), $f_S(S)$ is a crowding function (dimensionless) that limits the growth of seagrass at high densities due to self-shading, *R* is the respiration rate (g C g^{-1} DW d^{-1} or g C $shoot^{-1}$ d^{-1}), *E* is the dissolved organic carbon exudation rate (g C g^{-1} DW d^{-1} or g C $shoot^{-1}$ d^{-1}), and *m* is the mortality rate (d^{-1}). It is common to define the crowding function so that $f_S(S)$ approximates unity at low density (i.e., at low values of *S*) and $f_S(S)$ decreases as *S* increases. What is meant here by a "low" value of *S* will depend on the precise mathematical form of the crowding function chosen.

Eq. (1) is adapted from Kaldy (2012), and all loss processes described in Eq. (1) could be further split into losses from above- and below-ground biomass as needed. However, not all processes in Eq. (1) are included in all seagrass models; this equation is only provided here as a representative example of the modeling context in which our intertidal seagrass model is introduced (Section 2.2). In different models, seagrass *S* is quantified in either units of biomass (Jarvis et al., 2014; Turschwell et al., 2022) or shoot density (Adams et al., 2020; Carr et al., 2012), although these two quantities are positively correlated (Vieira et al., 2018). Similarly, different seagrass models assume different crowding functions $f_S(S)$, including the logistic growth function (Turschwell et al., 2022) or functions derived from light uptake based on geometric characteristics of self-shading (Baird et al., 2016); see Simpson et al. (2022) for other potentially relevant empirical

crowding functions. For the remainder of this paper, it will neither be necessary to specify the units in which seagrass is quantified nor define the form of the crowding function; our model results will be equally applicable to all choices of seagrass density units and crowding function.

Gross photosynthesis is the only process in Eq. (1) contributing positively to seagrass growth. It is common to rewrite $KP = \mu$ so that Eq. (1) becomes

$$\frac{dS}{dt} = \mu S f_S(S) - MS, \quad (2)$$

where μ is the per-capita growth rate (d^{-1}) at low seagrass densities (densities that make $f_S(S)$ approximate unity), and we have here grouped all loss terms into a per-capita loss rate M (d^{-1}). In the present paper, we focus solely on the per-capita growth rate at low seagrass densities due to gross photosynthesis, μ.

Previous seagrass models assume that the growth rate μ (and by extension, the photosynthesis rate P) depends on light, temperature and/or nutrients (Baird et al., 2016; Elkalay et al., 2003; Turschwell et al., 2022). If information about the cumulative interaction between these factors is known (i.e., synergistic, additive or antagonistic), this information can be included in the mathematical definition of μ (Adams et al., 2020). However, in the absence of such information, two common methods of modeling the effects of interacting factors on growth rate are to assume a multiplicative (Turschwell et al., 2022) or the law of the minimum (Baird et al., 2016) formulation in the mathematical definition of μ. In the present work we will use both multiplicative (Eq. (3)) and law of the minimum (Eq. (4)) formulations of μ, and consider the effects of two controlling factors on μ that have particular relevance in the intertidal zone - light and relative water content (RWC) of seagrass leaves,

'Multiplicative' formulation: $$\mu(I, \mathrm{RWC}) = \mu_{\max} f_I(I)\, f_{\mathrm{RWC}}(\mathrm{RWC}), \quad (3)$$

'Law of the minimum' formulation: $$\mu(I, \mathrm{RWC}) = \mu_{\max} \min\{ f_I(I), f_{\mathrm{RWC}}(\mathrm{RWC})\}. \quad (4)$$

In these equations, $\mu_{\max}$ is the maximum growth rate (d^{-1}), $f_I(I)$ is a unitless function representing the effect of irradiance (i.e., light, or more precisely, photosynthetically active radiation or PAR) on the growth rate, and $f_{\mathrm{RWC}}(\mathrm{RWC})$ is a unitless function representing the effect of RWC on the growth rate. Here, I (mol m^{-2} d^{-1}) is the daily PAR dose at the seagrass canopy, and RWC is written as a fraction (bounded between 0 and 1 inclusive). It is assumed that

the unitless functions $f_I(I)$ and $f_{\mathrm{RWC}}(\mathrm{RWC})$ can only take values between 0 and 1 inclusive, so that the growth rate μ satisfies $0 \leq \mu \leq \mu_{\max}$.

Although we are here only considering the effects of two controlling factors on the growth rate, each with its own unitless function in Eqs. (3) and (4), we point out that future applications of the model components we introduce could also incorporate other interacting factors (e.g., temperature, nutrients). These other factors could be incorporated in any subsequent models by the inclusion of appropriately defined additional functions within the multiplicative or law of the minimum formulation of the growth rate μ defined in Eqs. (3) and (4) respectively. We next describe each of the two unitless functions we focus on here (light and RWC) in further detail.

Various functional forms for the effect of irradiance on photosynthesis (and equivalently here, the growth rate) have been assumed in the literature (Jassby & Platt, 1976); there is not yet standardisation of this functional form in the marine biological modeling community (Tian, 2006). For the purposes of illustrating the new intertidal seagrass model components that we introduce in this paper, we chose the Michaelis-Menten function for $f_I(I)$ in the present work (Olesen & Sand-Jensen, 1993),

$$f_I(I) = \frac{\alpha I}{\mu_{\max} + \alpha I}, \quad (5)$$

where α ($d^{-1}/(mol\ m^{-2}\ d^{-1})$) indicates the efficiency of light utilisation for growth at low light.

2.2 Including intertidal effects: Modification of seagrass growth rate due to air-exposure

The photosynthesis rate of intertidal seagrasses is modified due to air exposure at low tides, and experimental data is available to parameterise this modification. Hence, we here describe mathematical relationships for how the seagrass growth rate may be altered by air exposure due to the loss of RWC in seagrass leaves when air exposed. The air-exposed responses of intertidal seagrasses are only triggered when the water depth drops to zero. The current conceptual understanding of the physiological processes for intertidal seagrasses when air-exposed and the associated equations considered in our model are shown in Figure 1.

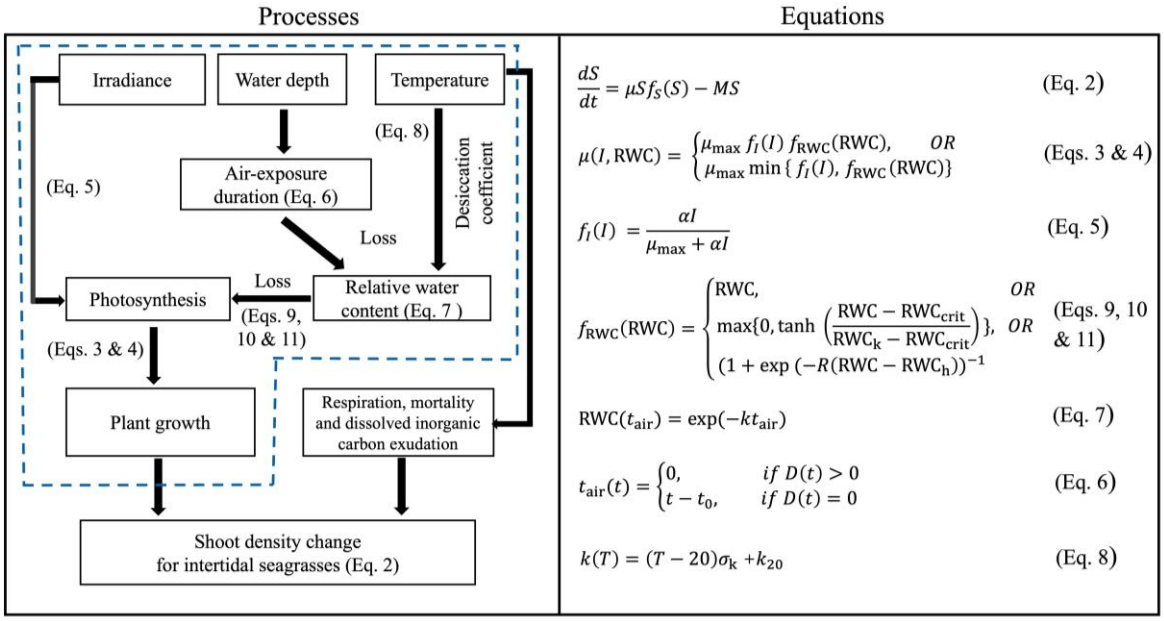

Figure 1 Schematic diagram of physiological processes and equations of intertidal seagrasses when air-exposed. The processes in the blue dashed box are quantitatively described in this study. The equations shown in the figure are numbered as in the main text.

2.2.1. The loss of relative water content

RWC of seagrass leaves generally decreases exponentially with time when seagrasses are exposed to air (Jiang et al., 2014; Papathanasiou et al., 2020; Shafer et al., 2007). For seagrasses present at the water depth D (m), the air-exposure duration t_{air} can be defined as a function of time t,

$$t_{\mathrm{air}}(t) = \begin{cases} 0, & \text{if } D(t) > 0, \\ t - t_0, & \text{if } D(t) = 0, \end{cases} \quad (6)$$

where t_0 marks the time when the water depth D first drops to zero during a single exposure-inundation cycle. Here, when the water depth becomes zero (D = 0), it signifies the emersion (i.e., air exposure) of seagrasses, while a positive water depth (D > 0) indicates the inundation of the seagrasses. For clarity, Figure 2 provides a visualization of how Eq. (6) represents the variation of air-exposure duration during a single exposure-inundation cycle.

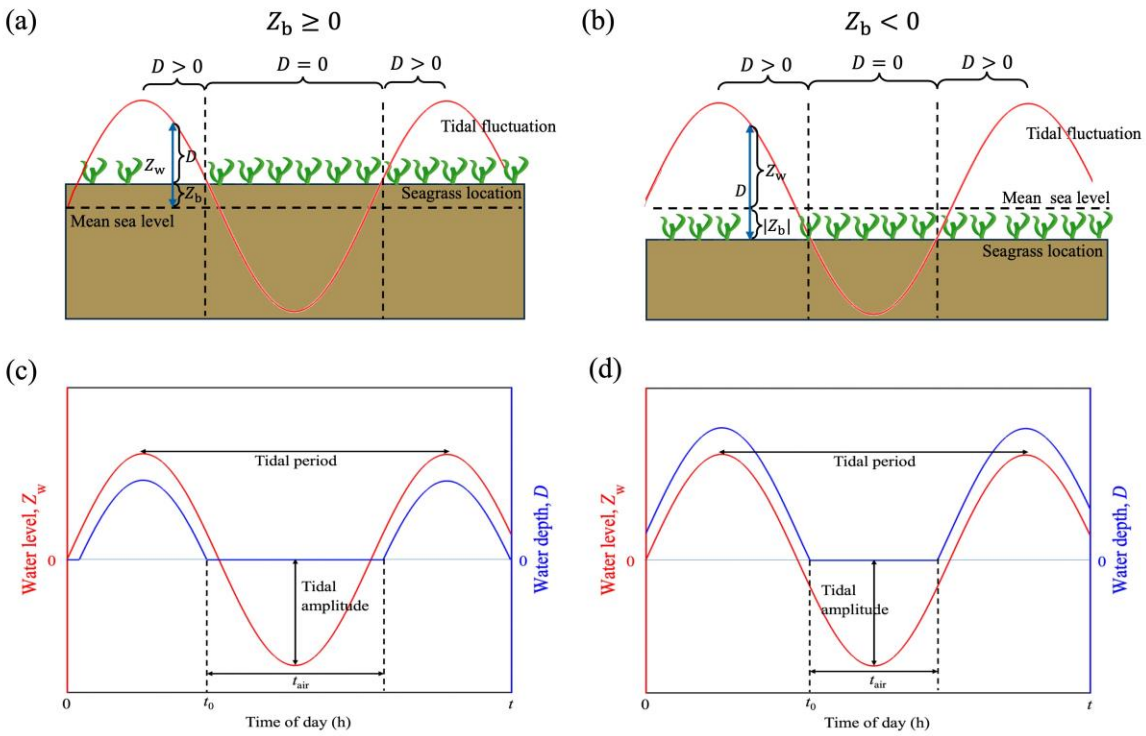

Figure 2 Variation of the water level $Z_w(t)$ and intertidal seagrass water depth $D(t)$ throughout the tidal cycle. Seagrass meadows may grow at (a) an elevation that is above mean sea level, i.e., $Z_b \geq 0$, or (b) at an elevation that is below mean sea level, i.e., $Z_b < 0$. In each of these two cases, the daily cycle of water level $Z_w(t)$ and intertidal seagrass water depth $D(t)$, can be assumed to approximately follow Eq. (12) and Eq. (13) respectively (introduced later in Section 2.3). The air-exposure duration t_{air} follows Eq. (6). For seagrass growing above mean sea level, this can result in daily time-series for $Z_w(t)$ and $D(t)$ following e.g., panel (c). For seagrass growing below mean sea level, this can result in daily time-series for $Z_w(t)$ and $D(t)$ following e.g., panel (d).

The exponential decline of RWC in seagrass leaves with air-exposure duration t_{air} can be subsequently modelled as (Jiang et al., 2014; Seddon & Cheshire, 2001; Shafer et al., 2007)

$$\mathrm{RWC}(t_{air}) = \exp(-kt_{air}), \quad (7)$$

where k is the desiccation coefficient (units of d^{-1}). As recovery of relative water content after re-submersion is expected to be relatively rapid (Azevedo et al., 2017), Eq. (7) inherently assumes that the fully hydrated state (i.e. RWC = 1) is instantly recovered for seagrass leaves after re-submersion. Thus, reduction in RWC only occurs when the water depth is zero (which

corresponds to $t_{\mathrm{air}} > 0$, see Eq. (6)), otherwise the seagrass leaves remain fully hydrated ($t_{\mathrm{air}} = 0$ in Eq. (6)).

Experimentally, the desiccation coefficient (k, in units of d^{-1}) has been found to vary with different seagrass species and is positively correlated with air temperature T (Seddon & Cheshire, 2001). Data for $k(T)$ has thus far only been collected at a small number of air temperatures; in the absence of other data, this relationship is assumed to be linear,

$$k(T) = (T - 20)\sigma_{\mathrm{k}} + k_{20}, \quad (8)$$

where σ_{k} (d^{-1} $^{\circ}\mathrm{C}^{-1}$) is the slope of the linear equation $k(T)$ when fitted to data for desiccation coefficient k versus air temperature T, and k_{20} (d^{-1}) is the desiccation coefficient at the air temperature of 20ºC. If seagrass leaf desiccation data is not collected at different air temperatures, then Eq. (8) cannot be used. Conversely, this equation could be superseded by a more complicated (i.e., nonlinear) function if data for seagrass leaf desiccation coefficients is available for a large range of air temperatures.

As an example, we determined the parameters σ_{k} and k_{20} for two seagrass species (*Posidonia australis* and *Amphibolis antarctica*) from best-fit calibration of Eq. (7) and (8) to data from the laboratory desiccation experiment described in Seddon & Cheshire (2001). Their experiment measured how RWC varies with t_{air} in *P. australis* and *A. antarctica* at four different air temperatures (18 ºC, 24 ºC, 28 ºC, 32 ºC). Figures S1-S3 in the Supporting Information show the plotted fits of Eq. (7) and (8) to the data, and Table S1 summarises the derived values of $k(T)$, σ_{k} and k_{20} from these plotted fits. In Table 1, we compile data from Seddon & Cheshire (2001), as well as many other studies, to show the wide range of desiccation coefficients observed at different air temperatures across various seagrass species and locations. It is clear that the desiccation coefficients exhibit substantial variability, ranging from ~ 8 d^{-1} to 260 d^{-1}.

Table 1

Summary of desiccation coefficients and corresponding air temperatures of intertidal/subtidal seagrasses from the literature.

Species [a]	**Location**	**Air temperature**	**Desiccation coefficient**	**Reference**

		(℃)	(d^{-1})	
Temperate				
Amphibolis antarctica	Spencer Gulf, South Australia	18	8.2[b]	Seddon & Cheshire (2001)
	Spencer Gulf, South Australia	24	10.6[b]	Seddon & Cheshire (2001)
	Spencer Gulf, South Australia	28	14.1[b]	Seddon & Cheshire (2001)
	Spencer Gulf, South Australia	32	14.0[b]	Seddon & Cheshire (2001)
	Swan Bay, Australia	NA	14.7[bc]	Pérez-Lloréns et al. (1994)
Cymodocea nodosa	Eleftheron Bay, Greece	24	61.9[b]	Papathanasiou et al. (2020)
Heterozostera tasmanica	Swan Bay, Australia	NA	21.8[c]	Pérez-Lloréns et al. (1994)
Posidonia australis	Spencer Gulf, South Australia	18	10.8[b]	Seddon & Cheshire (2001)
	Spencer Gulf, South Australia	24	12.9[b]	Seddon & Cheshire (2001)
	Spencer Gulf, South Australia	28	15.6[b]	Seddon & Cheshire (2001)
	Spencer Gulf, South Australia	32	16.8[b]	Seddon & Cheshire (2001)
	Swan Bay, Australia	NA	15.9[bc]	Pérez-Lloréns et al. (1994)
Nanozostera capensis (*Zostera capensis*)	Southern coast of Africa	25	62.7[cde]	Adams & Bate (1994)
Nanozostera	Padilla Bay, USA	22	193.0	Shafer et al.

japonica (*Zostera japonica*)				(2007)
Zostera marina	Padilla Bay, USA	22	46.1	Shafer et al. (2007)
Nanozostera muelleri (*Zostera muelleri*)	Swan Bay, Australia	NA	11.8[c]	Pérez-Lloréns et al. (1994)
Tropical/ subtropical				
Cymodocea rotundata	Ryukyu Islands, Japan	24.5	28.8	Tanaka & Nakaoka (2004)
	Ryukyu Islands, Japan	27	66.2	Tanaka & Nakaoka (2004)
Oceana serrulata (*Cymodocea serrulata*)	Ryukyu Islands, Japan	24.5	30.2	Tanaka & Nakaoka (2004)
	Ryukyu Islands, Japan	27	70.6	Tanaka & Nakaoka (2004)
Enhalus acoroides	Xincun Bay, China	24	20.2	Jiang et al. (2014)
	Xincun Bay, China	32	28.8	Jiang et al. (2014)
Halophila decipiens	East coast of Florida, USA	NA	230.4[b]	Kahn & Durako (2009)
Halophila johnsonii	East coast of Florida, USA	NA	259.2	Kahn & Durako (2009)
Halophila ovalis	Laem Yong Lam, Thailand	NA	10.7[e]	Wuthirak et al. (2016)
	Xincun Bay, China	24	40.3	Jiang et al. (2014)
	Xincun Bay, China	32	38.9	Jiang et al.

				(2014)
Thalassia hemprichii	Laem Yong Lam, Thailand	NA	7.5[e]	Wuthirak et al. (2016)
	Ryukyu Islands, Japan	24.5	18.7	Tanaka & Nakaoka (2004)
	Ryukyu Islands, Japan	27	37.4	Tanaka & Nakaoka (2004)

Note: [a] The name of seagrass species enclosed in brackets reflects the terminology previously used in the reference. We have revised this to reflect the current accepted name which is provided outside the brackets. [b] The data was collected from shallow subtidal seagrasses which could potentially be exposed to air at low tides, while all other data were from intertidal seagrasses; [c] The desiccation coefficient of this species was determined from the calibration of Eq. (7) to the data from corresponding references (Supporting Information Figure S4 shows the plotted fits of Eq. (7) to the data). [d] This desiccation rate value should be treated with caution, see the last plot within Supporting Information Figure S4. [e] These measurements were based on seagrass shoots, whereas all other measurements reported in this table were based on seagrass leaves. NA means data is not available in the literature.

2.2.2. The response of photosynthetic efficiency to RWC loss

In Section 2.2.1 we described how RWC of seagrass leaves is altered during the tidal cycle, which is similar to the desiccation module described in Azevedo et al. (2017). Here, we go one step further and connect the RWC changes through to seagrass dynamics via the effect of RWC on seagrass photosynthesis rate.

Several experimental studies have reported a gradual decrease in effective quantum yield (a measure of photosynthetic efficiency) in seagrasses as RWC reduces (Jiang et al., 2014; Kahn & Durako, 2009; Shafer et al., 2007). Here, we use these experimental findings to propose three alternative formulations for the unitless function $f_{\mathrm{RWC}}(\mathrm{RWC})$ which describes the effect of RWC on seagrass growth rate (see Eqs. (3) and (4)). As there is not yet sufficient quantitative information available in the literature for us to confidently propose models of recovery of photosynthetic efficiency after re-submersion, we assume that the photosynthetic efficiency is

instantly recovered for seagrass leaves after re-submersion. The precise form of the function $f_{\mathrm{RWC}}(\mathrm{RWC})$ is presumed here to be species-specific due to the species-specific differences in their tolerance to desiccation, although they may be location-specific as well (Section 3.1). The three alternative forms of $f_{\mathrm{RWC}}(\mathrm{RWC})$ that we propose are as follows:

Ⅰ. Linear model: In Kahn & Durako (2009) and Papathanasiou et al. (2020), the relationship between effective quantum yield and relative water content (RWC) for two temperate intertidal species, *H. johnsonii* and *C. nodosa*, was linear (Supporting Information Figure S5). This suggests a linear form of $f_{\mathrm{RWC}}(\mathrm{RWC})$ which we introduce as:

$$f_{\mathrm{RWC}}(\mathrm{RWC}) = \mathrm{RWC}. \tag{9}$$

Eq. (9) gives that $f_{\mathrm{RWC}}(\mathrm{RWC}) = 1$ when seagrass leaves are fully hydrated (RWC=1). The effective quantum yield is maximal, but usually less than one, when RWC=1 (Supporting Information Figure S5); this unavoidable inefficiency of the maximum effective quantum yield is scaled out in our mathematical formulation by the dimensionless form of $f_{\mathrm{RWC}}(\mathrm{RWC})$.

Ⅱ. Hyperbolic tangent model: In Jiang et al. (2014), the data for effective quantum yield versus RWC for tropical intertidal species *T. hemprichii* and *E. acoroides* were fitted to a standard hyperbolic tangent model. However, part of their data suggests that the value of $f_{\mathrm{RWC}}(\mathrm{RWC})$ could equal zero for some range of $\mathrm{RWC} > 0$ (see Supporting Information Figure S6), which is a behavior that is not possible using a standard hyperbolic tangent model unless a modification is made to its form. Thus, we introduced a modified hyperbolic tangent form of $f_{\mathrm{RWC}}(\mathrm{RWC})$ to fit the data of Jiang et al. (2014); after scaling out the maximum effective quantum yield, this modified function $f_{\mathrm{RWC}}(\mathrm{RWC})$ is:

$$f_{\mathrm{RWC}}(\mathrm{RWC}) = \max\left\{0, \tanh\left(\frac{\mathrm{RWC}-\mathrm{RWC}_{\mathrm{crit}}}{\mathrm{RWC}_{\mathrm{k}}-\mathrm{RWC}_{\mathrm{crit}}}\right)\right\}. \tag{10}$$

In Eq. (10), $\mathrm{RWC}_{\mathrm{crit}}$ (dimensionless) is the critical value of RWC below which the photosynthesis rate is zero, $\mathrm{RWC}_{\mathrm{k}}$ (dimensionless) is the value of RWC at which the photosynthesis rate is ~76% (when $\mathrm{RWC} = \mathrm{RWC}_{\mathrm{k}}$, $f_{\mathrm{RWC}}(\mathrm{RWC}) = \max\{0, \tanh(1)\} \approx 0.76$) of the maximum photosynthesis rate, and we enforce that the parameters $\mathrm{RWC}_{\mathrm{crit}}$ and $\mathrm{RWC}_{\mathrm{k}}$ must be non-negative. Mean parameter values for Eq. (10) fitted to *T. hemprichii* and *T. acoroides* data from Jiang et al. (2014) are provided in Supporting Information Table S2.

355

356 **Ⅲ Sigmoidal curve model:** In Shafer et al. (2007), the data of effective quantum yield and
357 RWC for temperate intertidal species *N. japonica* and *Z. marina* were fitted to a sigmoidal curve
358 model (see Supporting Information Figure S7). After scaling out the maximum effective
359 quantum yield, this model for $f_{\mathrm{RWC}}(\mathrm{RWC})$ can be written as:

360 $$f_{\mathrm{RWC}}(\mathrm{RWC}) = (1 + \exp(-R(\mathrm{RWC} - \mathrm{RWC_h}))^{-1}. \quad (11)$$

361 where R (dimensionless) is the shape parameter of the fitted sigmoidal curve model, and $\mathrm{RWC_h}$
362 (dimensionless) is the value of RWC that gives half of the maximum photosynthesis rate. Mean
363 parameter values for Eq. (11) fitted to *N. japonica* and *Z. marina* data from Shafer et al. (2007)
364 are provided in Supporting Information Table S2.

365

366 2.3 Simulating the intertidal cycle of air exposure and inundation

367 Now that a proposed modeling framework for intertidal seagrass has been fully described
368 (Section 2.1, summarised in Figure 1), we next sought to simulate models within this framework
369 to explore what these models predict. This requires simulation of the intertidal seagrass response
370 to dynamically changing environmental conditions, including daily fluctuations in water depth,
371 irradiance and air temperature. Daily variation of environmental conditions can be quite
372 complex; hence, it will be useful here to define "minimum realistic" models (Geary et al., 2020)
373 of the external environmental conditions for the purposes of exploring the consequences of our
374 intertidal seagrass model formulations. Here, we describe minimum realistic models for daily
375 fluctuations in water depth, irradiance and air temperature conditions, and later in Section 2.4.2
376 we describe how we will use these models as environmental forcings for simulating our intertidal
377 seagrass model.

378

379 First, the tidal cycles affect the water depth in the intertidal seagrass meadows, leading to
380 periodic air exposure of seagrasses. We assumed that air exposure of seagrasses was forced by
381 the M2 and S2 tidal constituents (i.e., the dominant constituents that lead to typical spring-neap
382 tidal cycles) in the intertidal zones. Therefore, two superimposed cosine curves with different
383 amplitudes and periods representing the M2 and S2 tidal constituents (Balke et al., 2016) were
384 simulated to determine the water level relative to mean sea level,

385 $$Z_{\mathrm{w}}(t) = A_{\mathrm{M2}} \times \cos\left(\frac{2\pi t}{T_{\mathrm{M2}}}\right) + A_{\mathrm{S2}} \times \cos\left(\frac{2\pi t}{T_{\mathrm{S2}}}\right), \quad (12)$$

where $Z_{\mathrm{w}}(t)$ is the water level (m) relative to mean sea level at time t (d), A_{M2} is the amplitude of the M2 tidal constituent (m), T_{M2} is the period of the M2 tidal constituent (d), A_{S2} is the amplitude of the S2 tidal constituent (m), and T_{S2} is the period of the S2 tidal constituent (d). Consequently, the water depth D (m) at an intertidal seagrass meadow of interest is dictated by the changes in water level relative to meadow elevation,

$$D = \begin{cases} Z_{\mathrm{w}} - Z_{\mathrm{b}}, & if\ Z_{\mathrm{w}} > Z_{\mathrm{b}}, \\ 0, & if\ Z_{\mathrm{w}} \leq Z_{\mathrm{b}}, \end{cases} \tag{13}$$

where Z_{b} is the elevation of seagrass meadow relative to mean sea level (m). The relationship between water level Z_{w} and intertidal seagrass water depth D throughout the tidal cycle is visualised in Figure 2c & 2d.

Second, a minimum realistic model for daily light fluctuations is as follows. The within-daily water surface light $I_{\mathrm{s}}(t)$ (in units of mol m^{-2} d^{-1}) varies sinusoidally during the day, peaking at solar noon (i.e., 12 hours after solar midnight). However, the water surface light $I_{\mathrm{s}}(t)$ must also be zero at night. This can be accomplished by using a sinusoidal curve for $I_{\mathrm{s}}(t)$ that is truncated to be non-negative according to Johnson & Thornley (1984) and Adams et al. (2020),

$$I_{\mathrm{s}}(t) = \begin{cases} 0, & if\ t \leq t_{\mathrm{rise}} \text{ or } t \geq t_{\mathrm{rise}} + L, \\ \frac{\pi}{2L} \overline{I_{\mathrm{s}}} \sin\left(\frac{\pi}{L}(t - t_{\mathrm{rise}})\right), & if\ t_{\mathrm{rise}} \leq t \leq t_{\mathrm{rise}} + L, \end{cases} \tag{14}$$

where $\overline{I_{\mathrm{s}}}$ is the daily average water surface light (mol m^{-2} d^{-1}), t is the time since solar midnight (d), t_{rise} is the daily sunrise time (d), and L is the day length (from sunrise to sunset) (d). Because tidal inundation of the seagrasses reduces the light they receive, the benthic light $I(t)$ experienced by the seagrasses can then be calculated from the Beer-Lambert law (Kirk, 1985),

$$I(t) = I_{\mathrm{s}}(t)\, e^{-K_{\mathrm{d}} D(t)}, \tag{15}$$

where K_{d} is the light attenuation coefficient in the water column (m^{-1}), assumed here to be spatiotemporally constant for simplicity.

Finally, daily fluctuations in air temperature $T_{\mathrm{air}}(t)$ (in units of $^{\mathrm{o}}$C) can be coarsely approximated by a sinusoidal variation that peaks at a maximum air temperature some time $t_{\emptyset}$ (in d) after solar noon (Adams et al., 2020),

$$T_{\mathrm{air}}(t) = \overline{T} - \Delta T \cos(2\pi(t - t_{\emptyset})), \tag{16}$$

where $\bar{T}$ is the mean daily air temperature (℃) and ΔT (℃) is the maximum variation of daily air temperature from its mean value. A visualisation of Eqs. (14) and (16) is provided in Supporting Information Figure S8.

2.4 Model simulations

Using the data-calibrated intertidal seagrass model formulations and minimum realistic models for daily fluctuating environmental parameters introduced in the previous sections, we produced model simulations to explore both the applicability and consequences of the introduced formulations. First, we compared our data-calibrated formulations of seagrass photosynthetic efficiency reduction due to desiccation (captured by the function $f_{\mathrm{RWC}}(\mathrm{RWC})$) to previously published experimental results for the same seagrass species at different locations and for the same and different tissue types (i.e., leaf versus shoot). Further explanation of this comparison is provided in Section 2.4.1. Second, seagrass growth rates were simulated under a variety of physiological process assumptions and environmental scenarios to identify generalisable conclusions obtained from our introduced intertidal seagrass model formulations (Section 2.4.2).

2.4.1. Investigating the applicability of a parameterised intertidal seagrass model to other locations and other seagrass tissue types

We compared our data-calibrated formulations of seagrass photosynthetic efficiency reduction due to desiccation ($f_{\mathrm{RWC}}(\mathrm{RWC})$) to data from additional experimental studies (Kim et al., 2020; Park et al., 2016). The purpose of this analysis was to identify the applicability of $f_{\mathrm{RWC}}(\mathrm{RWC})$ functions parameterised by data from a seagrass species at a particular location and with a particular tissue type, to the same species (1) in different locations, and (2) for the same and different tissue types. This is an important modeling question to consider, as environmental models are often parameterised using data from one location and applied to another location. We sought to understand the validity of such an application for our introduced intertidal seagrass model formulations.

To accomplish this, we simulated the relationship between photosynthetic efficiency scaled by its maximum, i.e., $f_{\mathrm{RWC}}(\mathrm{RWC})$, and air-exposure duration t_{air}, using Eqs. (7) and (11)

parameterised to data (Supporting Information Figure S7) obtained for *Z. marina* and *N. japonica* leaves in Padilla Bay, USA (Shafer et al., 2007). We compared these predictions of $f_{\mathrm{RWC}}(\mathrm{RWC})$ to measured photosynthetic efficiency changes for *Z. marina* and *N. japonica* reported in two experimental studies that were both carried out in the southern coast of South Korea (Kim et al., 2020; Park et al., 2016). Two datasets for *Z. marina* (Park et al., 2016) were available - both were for seagrass shoots, but at different sites within the southern coast of South Korea (Aenggang Bay and Koje Bay). Two datasets for *N. japonica* (Kim et al., 2020) were also available – both were measured at Koje Bay, but for different seagrass tissues (leaves and shoots). Hence these datasets allowed us to examine the applicability of $f_{\mathrm{RWC}}(\mathrm{RWC})$ formulations parameterised for seagrass species in one location to the same seagrass species in other locations and for the same and different seagrass tissues.

2.4.2. Investigating the dependence of intertidal seagrass growth rate on model assumptions and environmental conditions

We then conducted a plethora of simulation scenarios for the introduced growth rate function $\mu(I, \mathrm{RWC})$ using Eqs. (6)-(11), with environmental forcings provided by daily fluctuations in water depth, light, and air temperature (Eqs. (12)-(16)). These scenarios allowed us to investigate (1) what effects do inclusion of seagrass physiological responses to intertidal processes have on their growth rates (i.e. including the factor $f_{\mathrm{RWC}}(\mathrm{RWC})$ in seagrass models), (2) what differences in growth rates arise from different model assumptions (i.e., the assumption of which form of $f_{\mathrm{RWC}}(\mathrm{RWC})$ (Eq. (9)-(11)); and the assumption of whether cumulative stressors interact multiplicatively (Eq. (3)) or if seagrass respond only to the strongest stressor (Eq. (4)), and (3) the effects of water turbidity, meadow elevation and tidal range on intertidal seagrass growth rate. For the remainder of this section, we detail what simulations were performed to undertake these investigations. In all simulations, the total period simulated was 15 d to cover an entire spring-neap cycle, and we assumed that the within-daily fluctuations of light and air temperature did not change from day to day.

Baseline scenario. We first describe a "Baseline" scenario for our simulations, which represents a specific set of environmental and seagrass growth characteristics that all our other "testing"

scenarios are compared to. In the Baseline scenario, the cumulative effect of light deprivation and desiccation on seagrass growth $\mu(I, \text{RWC})$ was assumed to follow the multiplicative formulation (Eq. (3)). In some of our testing scenarios described later, we also examined the law of the minimum formulation given in Eq. (4).

For the Baseline scenario, we parameterised the model simulations for the common intertidal seagrass genera *Zostera*, using parameters drawn (where possible) from data for intertidal *N. japonica* meadows in the Yellow River Estuary (YRE), China. This choice of species and location for model parameterisation is relatively arbitrary since we are not particularly interested in the precise quantitative predictions of any individual simulation; instead, we are here primarily interested in comparing simulations between scenarios. *N. japonica* is a reasonable species choice for this purpose because it is one of the most widely distributed seagrass species in China's coastal areas. Similarly, the YRE is a reasonable location choice because it contains the largest habitat of *N. japonica* in China (Zhou et al., 2022), where we have performed extensive field monitoring and experiments (Wang et al., 2022; Wang et al., 2021).

Hence, we drew parameters for the daily fluctuations of air temperature and light from a mixture of published (Zhang et al., 2019) and unpublished data for YRE (Table 2). Specifically, light and air temperature parameters were obtained from monitoring data from June to August in a typical growing season of the intertidal seagrass meadows in the YRE. Due to the lack of physiological data for *N. japonica* available at YRE, seagrass photosynthesis responses to RWC were instead obtained from data for *N. japonica* growing in the similar temperate region of Padilla Bay, USA (Shafer et al., 2007), for which the sigmoidal curve model for $f_{\text{RWC}}(\text{RWC})$ given in Eq. (11) has already been fitted in the present study (Supporting Information Table S2 and Supporting Information Figure S7). Similarly, we could not find a parameterisation of the photosynthesis-irradiance relationship for *N. japonica*, and thus seagrass growth responses to light were parameterised from the related species *Z. marina* growing in Danish waters (Olesen & Sand-Jensen, 1993) which possess a similar temperate climate to the YRE.

Table 2

Modeling variables and parameters for the Baseline scenario.

	Description	Value	Unit	Reference
Variables				
μ	Growth rate of seagrass	-	d^{-1}	-
k	Desiccation coefficient	-	d^{-1}	-
RWC	Relative water content of seagrass leaves	-	-	-
t_{air}	Air-exposed duration	-	d	-
t_0	The first time when the water depth is zero during a single exposure-inundation cycle	-	d	
D	Water depth experienced by the seagrass	-	m	-
Z_{w}	Water level relative to mean sea level	-	m	-
I_{s}	Water surface light	-	mol m^{-2} d^{-1}	-
I	Benthic light	-	mol m^{-2} d^{-1}	-
T_{air}	Air temperature	-	°C	-
Parameters				
μ_{max}	Maximum seagrass growth rate	0.04[a]	d^{-1}	Olesen & Sand-Jensen (1993)
α	Efficiency of light utilisation for seagrass growth at low light	0.01[a]	d^{-1}/ (mol m^{-2} d^{-1})	Olesen & Sand-Jensen (1993)
k_{20}	Desiccation coefficient at the air temperature of 20ºC	11.6	d^{-1}	This study (Supporting Information Table S1) calculated from Seddon & Cheshire (2001)
σ_{k}	Rate of change of desiccation	0.5	d^{-1} °C^{-1}	This study

	coefficient with air temperature			(Supporting Information Table S1) calculated from Seddon & Cheshire (2001)
$\mathrm{RWC_h}$	The value of RWC that attains half of the effective quantum yield for *N.japonica* in sigmoidal curve model of $f_{\mathrm{RWC}}(\mathrm{RWC})$	0.4	-	This study (Supporting Information Table S2) calculated from Shafer et al. (2007)
R	Shape parameter in sigmoidal curve model of $f_{\mathrm{RWC}}(\mathrm{RWC})$	15.0	-	This study (Supporting Information Table S2) calculated from Shafer et al. (2007)
A_{M2}	Amplitude of M2 tidal constituent	0.6	m	Fan et al. (2020)
	Amplitude of S2 tidal constituent	0.2	m	Fan et al. (2020)
T_{M2}	Period of M2 tidal constituent	0.5175	d	Constant value
T_{S2}	Period of S2 tidal constituent	0.5	d	Constant value
Z_{b}	Elevation of seagrass meadow relative to mean sea level	0	m	Assumed in this study
$\overline{I_{\mathrm{s}}}$	Daily average water surface light	60	mol m^{-2} d^{-1}	Zhang et al. (2019)

K_{d}	Light attenuation coefficient in the water column	0.05	m^{-1}	Christensen et al. (2004)
t_{rise}	Daily sunrise time	0.2708	d	Our unpublished data
L	Day length	0.5	d	Assumed in this study
$\bar{T}$	Mean daily air temperature	25	℃	Zhang et al. (2019)
ΔT	Daily air temperature from its mean value	5	℃	Zhang et al. (2019)
$t_{\emptyset}$	Time between solar noon and when the maximum air temperature occurs in the afternoon	0.083	d	Our unpublished data

[a] The values of $\mu_{\max}$ and α reported in Olesen & Sand-Jensen (1993) were 43.1 mg g^{-1} d^{-1} and 0.72 mg g^{-1} d^{-1}/(μmol m^{-2} s^{-1}), respectively. We performed unit conversions to obtain $\mu_{\max} = 0.04$ d^{-1} and $\alpha = 0.01$ d^{-1}/ (mol m^{-2} d^{-1}), respectively.

Because we wanted to include the effects of air temperature-dependent desiccation (Eq. (8)) in our explorative simulations, and the only data available for this relationship are for two species (temperate *P. australis* and *A. antarctica*, see Supporting Information Table S1), we parameterised air temperature-dependent desiccation (Supporting Information Figure S1) in the Baseline scenario based on *P. australis* (Seddon & Cheshire, 2001) due to this species' similar climatic zone to *N. japonica*. Whilst the reported desiccation coefficient for *N. japonica* is closer to the coefficients for *P. australis* than *A. antarctica* (Table 1), we also acknowledge that the difference in these coefficients exceeds an order of magnitude. We thus reiterate here that the purpose of our simulations is to explore consequences of the model behavior rather than parameterise the intertidal seagrass model precisely for *N. japonica*, as air temperature-dependent desiccation coefficient information is not currently available for this species.

Finally, we chose "semi-diurnal" tides and "microtidal" conditions for the Baseline scenario, since the YRE is a microtidal estuary dominated by semi-diurnal tides (Zhou et al., 2022). Semi-diurnal tides indicate that two high tides and two low tides of similar size occur every day, and microtidal conditions indicate a daily tidal range of less than 2 m. Parameterisation of the amplitude for tidal constituents yielding these microtidal conditions was obtained from the field monitoring data in the YRE (Fan et al., 2020). The tidal periods for M2 and S2 constituents are constant. To assess the applicability of our model in the Baseline scenario, which explores the physiological responses of intertidal seagrass to desiccation while minimizing the impact of light availability, we assumed a low turbidity level (represented by water-column light attenuation coefficient K_d = 0.05 m^{-1}), which is the lowest value for seagrass meadows we could find in the literature (Christensen et al., 2004). In the Baseline scenario we also assumed a meadow elevation at mean sea level, Z_b = 0 m, to represent the intermediate intertidal zone. In some of our testing scenarios described later, we also examined the effects of different meadow elevations and water turbidity on intertidal seagrass growth. The full parameterisation of the Baseline scenario is given in Table 2.

Testing scenarios. The testing scenarios were divided into four groups (labelled as Groups I, II, III and IV, see Supporting Information Table S3), and these scenarios were compared to the Baseline scenario. Simulations in Group I aimed to examine the effects of including air-exposure responses in seagrass growth models (i.e., $\mu(I)$ versus $\mu(I, \mathrm{RWC})$), as well as the effects of different model assumptions. The model assumptions compared were the different forms of $f_{\mathrm{RWC}}(\mathrm{RWC})$ - linear (Eq. (9)) versus hyperbolic tangent (Eq. (10)) versus sigmoidal (Eq. (11)) - and whether $\mu(I, \mathrm{RWC})$ follows a multiplicative formulation (Eq. (3)) or law of the minimum formulation (Eq. (4)). For testing scenarios that used the hyperbolic tangent form of $f_{\mathrm{RWC}}(\mathrm{RWC})$, parameters for *T. hemprichii* at the air temperature of 24°C (similar climatically to YRE, Supporting Information Table S2) were used. All testing scenarios in Group I were otherwise the same as the Baseline scenario.

Simulations in Groups II aimed to examine the effects of water turbidity (five turbidity levels from low to high) and meadow elevation (intertidal versus subtidal versus supratidal zones). More specifically, the five levels of water turbidity tested were K_d = 0.05 m^{-1}, 0.5 m^{-1}, 1 m^{-1}, 1.5

552 m^{-1} and 2 m^{-1}, as they represent a range of K_d values (0.05 to 2 m^{-1}) corresponding to a
553 reasonable range of irradiances that seagrasses may be able to tolerate (Christensen et al., 2004).
554 We considered different zones along the intertidal gradient by simulating a continuous gradient
555 of meadow elevations ranging from 3 m below mean sea level to 3 m above mean sea level (i.e.,
556 Z_b ranging from -3 m to 3 m). Three different zones were subsequently categorized based on
557 tidal range as follows: the intertidal zone spans the area between the low and high tides and is
558 affected by daily tidal cycle; the subtidal zone is situated below the low tides and serves as a
559 permanently submerged zone; and the supratidal zone is positioned above the high tides and is
560 not inundated at any time. This continuous gradient of meadow elevations was simulated at the
561 same five water turbidity levels.
562
563 Simulations in Group III were identical to simulations in Group II, except that all Group II
564 simulations were for microtidal conditions, and all Group III simulations were for mesotidal
565 conditions (i.e., daily tidal range between 2 m and 4 m). Similarly, Group IV simulations were
566 identical to Group II simulations, except that Group IV simulations were performed for
567 macrotidal conditions (i.e., daily tidal range greater than 4 m). A larger tidal range represents a
568 wider intertidal zone and stronger tidal effects on intertidal seagrasses. The parameterisations of
569 mesotidal and macrotidal conditions were obtained from studies on temperate intertidal Zostera
570 meadows located in the north-western Portuguese Coast (Azevedo et al., 2017) and French
571 Atlantic Coast (Toublanc et al., 2015), respectively (see Supporting Information Table S3
572 caption for full details). Hence, the Baseline scenario and testing scenarios in Groups II, III and
573 IV collectively provide a multifactorial simulated comparison of the effects of meadow
574 elevation, water turbidity and tidal conditions on intertidal seagrass growth. This final targeted
575 set of simulations allowed us to investigate (1) the trade-off between the increased light
576 experienced further up the depth gradient (beneficial for seagrasses) and the increased
577 desiccation further up the depth gradient (detrimental for seagrasses), and (2) how this trade-off
578 depends on water turbidity and tidal conditions. All baseline and testing scenarios for the model
579 application are detailed in Supporting Information Table S3. All model simulations and figure
580 visualizations were performed in MATLAB (R2022a).
581 **3 Results**

582 3.1 The variability of seagrass photosynthetic responses to air exposures

583 Our first finding is that there is considerable variability in the photosynthetic responses of
584 seagrasses to air exposures among locations and seagrass tissues. Specifically, among the same
585 *Z. marina* species at distinct locations, substantial differences are evident in the relationship
586 between seagrass photosynthetic efficiency and air-exposure duration, as observed in the results
587 of experimental studies in Koje Bay and Aenggang Bay on the southern coast of South Korea
588 (Figure 3a). Notable distinctions also arise for *N. japonica* when comparing our modeling results
589 with experimental data from Padilla Bay in the USA and Koje Bay in South Korea, respectively
590 (Figure 3b). Furthermore, an examination of different seagrass tissue types reveals a higher
591 desiccation tolerance in entire shoots compared to leaves for *N. japonica*, as indicated by
592 experimental data (Figure 3b). The variability becomes more pronounced when comparing our
593 modeled results and experimental data for *Z. marina*, considering both different tissue types and
594 locations (Figure 3a). This suggests that it is difficult to transfer a model parameterised at one
595 location/for one seagrass tissue to another location/tissue due to the influence of environmental
596 conditions such as light, temperature, wind, humidity, soil properties, etc. in the field as well as
597 the different water retention ability of seagrass tissues (Kim et al., 2020; Suykerbuyk et al.,
598 2018).

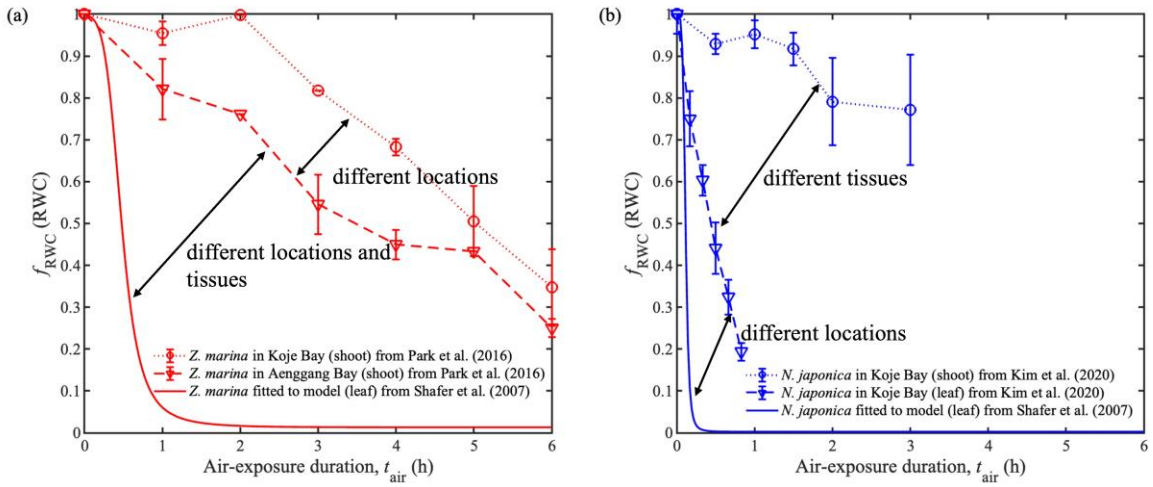

599

600 **Figure 3** Relationship between seagrass photosynthetic efficiency and air-exposure duration for
601 (a) *Z. marina* and (b) *N. japonica.* Notice that there are substantial differences in RWC versus
602 air-exposure duration for the same species at different locations and in different tissues (shoot
603 vs leaf).

3.2 Physiological responses of intertidal seagrasses when air-exposed

Our finding is that desiccation has a substantial effect on seagrass growth rate, thus justifying the new formulations for growth rate $\mu(I, \mathrm{RWC})$ introduced in the present work, as follows. In our Baseline scenario of simulating intertidal seagrasses (Eqs. (6) - (11), (12) - (16) parameterized using Table 2), the modelled water depth fluctuates throughout the spring-neap tidal cycle (Figure 4a). The intertidal seagrasses are subject to air exposure at low tides twice a day, each lasting for nearly 6 hours (Supporting Information Figure S9a), with the RWC dropping to low values in each exposure period (Supporting Information Figure S9b). As a result, the seagrass growth rate in the Baseline scenario, which is dependent on both light and RWC ($\mu(I, \mathrm{RWC})$), fluctuates throughout the spring-neap tides (Figure 4b). On the other hand, if the seagrass growth rate depends solely on light ($\mu(I)$), the fluctuation of this growth rate due to tidal-induced light deprivation is very minor (Figure 4c). Furthermore, the modelled average growth rate (represented by the dashed lines in Figure 4) is substantially lower for $\mu(I, \mathrm{RWC})$ than for $\mu(I)$.

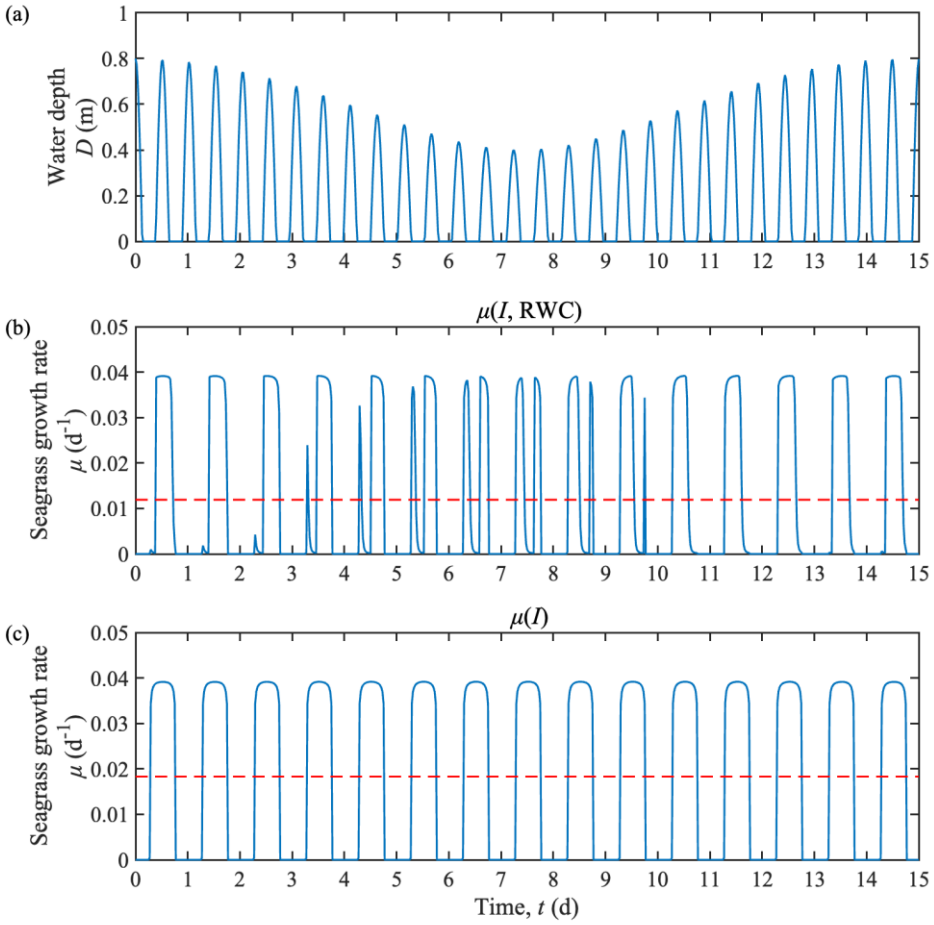

Figure 4 (a) Modelled water depth over 15 d in the Baseline scenario (Table 2); Predicted seagrass growth rate over 15 d for (b) growth rate dependent on light and RWC (Baseline scenario, see Table 2) and (c) growth rate only dependent on light (first testing scenario in Group I, see Supporting Information Table S3). The red dashed line represents the mean value of the growth rate over the 15-d simulation. Notice that accounting for desiccation causes the prediction of the mean growth rate to be substantially lower (compare red dashed lines between (a) and (b)).

Next, we investigated how the cumulative effect of air-exposure duration and light deprivation on seagrass growth rate is mediated by the multiplicative or law of the minimum formulation representing these cumulative stressors. To accomplish this, we performed simulations that exactly matched the Baseline scenario (Table 2) or possessed minor modifications of this scenario. More specifically, for a single exposure-inundation cycle, we adopted two constant values of benthic light irradiance in the model, i.e. one below and one above the saturating irradiance (15 mol m^{-2} d^{-1} in Park et al. (2021)), and we selected a single exposure-inundation cycle during spring tide in our model scenarios (Figure. 5).

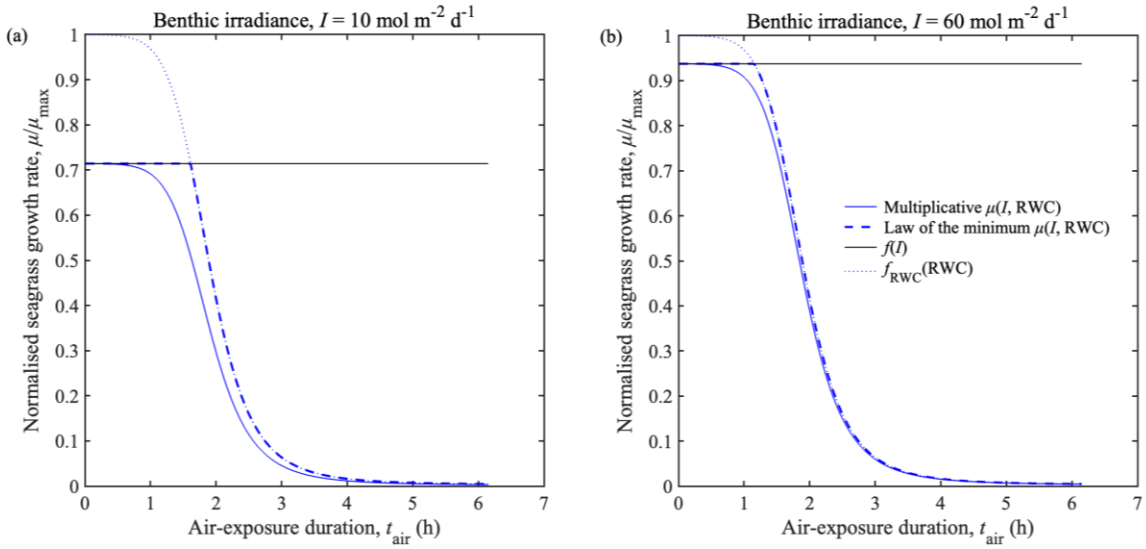

Figure 5 The relationship between the normalized growth rate ($\mu/\mu_{\max}$) and air-exposure duration (t_{air}) for two seagrass growth functions with sigmoidal curve $f_{\text{RWC}}(\text{RWC})$ under two light irradiance conditions: (a) 10 mol m^{-2} d^{-1} and (b) 60 mol m^{-2} d^{-1}. These simulations are equivalent to, or slight modifications of the Baseline scenario described in Table 2. Notice that the growth rate always reduces with air- exposure duration faster with the multiplicative

formulation (solid blue line) is assumed, compared to the law of the minimum formulation (dashed blue line), but this effect is reduced as benthic irradiance increases (e.g., from panel (a) to (b)).

We utilized the normalized growth rate ($\mu/\mu_{\max}$) to compare the differences between growth rate scenarios using the multiplicative or law of the minimum formulation for *Zostera* spp. with sigmoidal $f_{\mathrm{RWC}}(\mathrm{RWC})$. The results (Figure 5) reveal that, regardless of the light level, when applying the multiplicative formulation (solid blue lines), the growth rate begins to decline earlier in response to air exposure than when applying the law of the minimum formulation (dashed blue lines). However, when the benthic light irradiance is 60 mol m^{-2} d^{-1} (well above the saturating irradiance, Figure 5b), the differences in growth rate response to air exposure between multiplicative and law of the minimum formulation scenarios are smaller than when the benthic irradiance is below saturation (10 mol m^{-2} d^{-1}, Figure 5a). The law of the minimum formulation consistently yields a more optimistic prediction of seagrass growth rate than the multiplicative formulation, and the difference between the predictions of these two formulations tends to widen when multiple stressors (e.g., desiccation and light deprivation) are expected to have substantial detrimental impacts on seagrass growth.

3.3 Species-specific effects on intertidal seagrass growth

We next ran simulations with three different functional forms $f_{\mathrm{RWC}}(\mathrm{RWC})$ for the effect of seagrass tissue relative water content on seagrass photosynthetic efficiency to examine the impact of desiccation tolerance of different seagrass species on their growth rates (Baseline and Group I scenarios, see Supporting Information Table S3). The results show that the hyperbolic tangent model assumed for $f_{\mathrm{RWC}}(\mathrm{RWC})$ yielded a higher predicted 15d-averaged growth rate of seagrass in comparison to other functional forms of $f_{\mathrm{RWC}}(\mathrm{RWC})$ (Figure 6). This suggests that the function $f_{\mathrm{RWC}}(\mathrm{RWC})$ characterizing the desiccation tolerance of species constitutes an important factor. The reason that the hyperbolic tangent model for $f_{\mathrm{RWC}}(\mathrm{RWC})$ yields a higher overall growth rate for intertidal seagrass is because mathematically it predicts a higher photosynthetic efficiency $f_{\mathrm{RWC}}(\mathrm{RWC})$ at all values of RWC < 1 compared to the other two functional forms (linear and sigmoidal curve). The difference in $f_{\mathrm{RWC}}(\mathrm{RWC})$ between the hyperbolic tangent model and the other two forms are particularly large at high RWC values

671 which are experienced by the seagrasses soon after air exposure begins. Supporting Information
672 Figure S11 demonstrates that this causes a delay in the reduction of seagrass growth rate
673 following air exposure if the hyperbolic tangent model of $f_{\mathrm{RWC}}(\mathrm{RWC})$ is assumed (green lines in
674 Supporting Information Figure S11); this delay in the reduction of seagrass growth rate
675 following air exposure is substantially reduced for the other two functional forms of $f_{\mathrm{RWC}}(\mathrm{RWC})$
676 (blue and red lines in Supporting Information Figure S11). Each $f_{\mathrm{RWC}}(\mathrm{RWC})$ was obtained from
677 different seagrass species (Supporting Information Figure S5-S7), and thus it may be the case
678 that species-specific functional forms of $f_{\mathrm{RWC}}(\mathrm{RWC})$ play a key role in determining the seagrass
679 species tolerance to desiccation.
680
681 Meanwhile, there were no substantial differences between average growth rates for functions that
682 followed the multiplicative or law of the minimum formulations with the same $f_{\mathrm{RWC}}(\mathrm{RWC})$.
683 Note that these growth rates were calculated under very high light conditions (60 mol m^{-2} d^{-1}as
684 assumed in the Baseline scenario), which led to this small difference between the multiplicative
685 and law of the minimum formulations (see Figure 5b and the related discussion). At lower
686 irradiances (10 mol m^{-2} d^{-1}), these differences increase marginally (see Supporting Information
687 Figure S10), and the difference between functional forms of $f_{\mathrm{RWC}}(\mathrm{RWC})$ tends to have a larger
688 effect on the growth rate (Supporting Information Figure S11a).
689

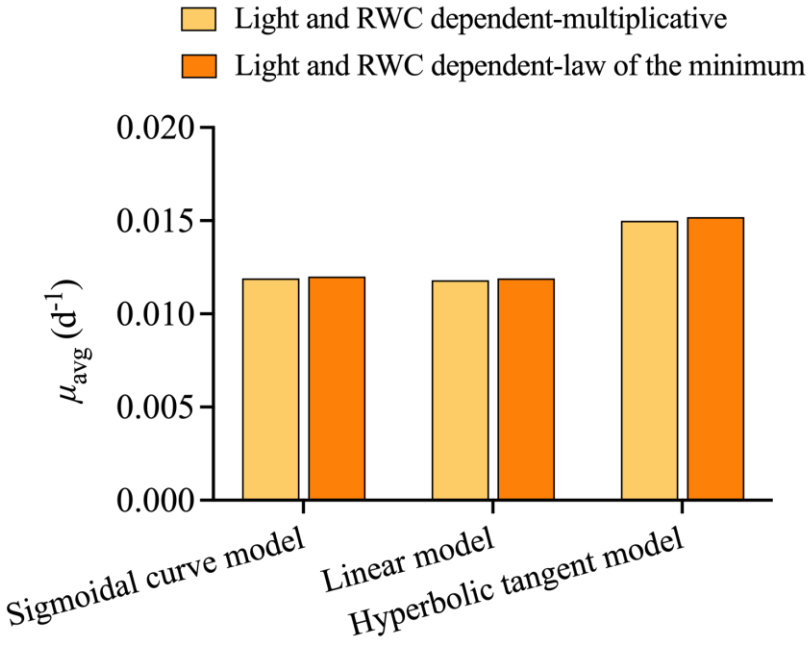

690

Figure 6 The results of modelled average growth rate (μ_{avg}) during the simulation period of 15 d for light and RWC dependent growth rate followed the multiplicative or law of the minimum formulation with the three types of $f_{\mathrm{RWC}}(\mathrm{RWC})$ defined in Eq. (9)-(11). Notice that mean growth rates are always predicted to be higher if the hyperbolic tangent form of $f_{\mathrm{RWC}}(\mathrm{RWC})$ (i.e., Eq. (10) is assumed).

3.4 Intertidal seagrass growth along vertical gradient under different tidal range condition

Within a 15-d simulation in different modeling scenarios (Baseline and Groups II, III and IV, see Section 2.4.2 and Supporting Information Table S3 for full details), we compared the 15d-averaged predictions of (1-$f_I(I)$) and (1-$f_{\mathrm{RWC}}(\mathrm{RWC})$) to illustrate, and as metrics of, the light deprivation and desiccation stress on the intertidal seagrass growth, respectively. The results show that within a specific tidal range area in the intertidal zones, light deprivation stress gradually decreases and desiccation stress increases as meadow elevation increases (compare red and blue lines in Figure 7 a, c & e). Meanwhile, the light deprivation stress on seagrass growth dramatically increases as the water turbidity level rises (compare different red lines in Figure 7a, c & e), leading to more substantial variations along the vertical gradient. In the subtidal zones, light deprivation is the predominant stress on seagrass growth, which gradually decreases as elevation increases, and desiccation stress is absent in these zones. In contrast, desiccation is the dominant stressor impacting seagrass growth in the supratidal zones, where light deprivation stress is minimal (only limited by the efficiency of light utilisation for seagrass growth).

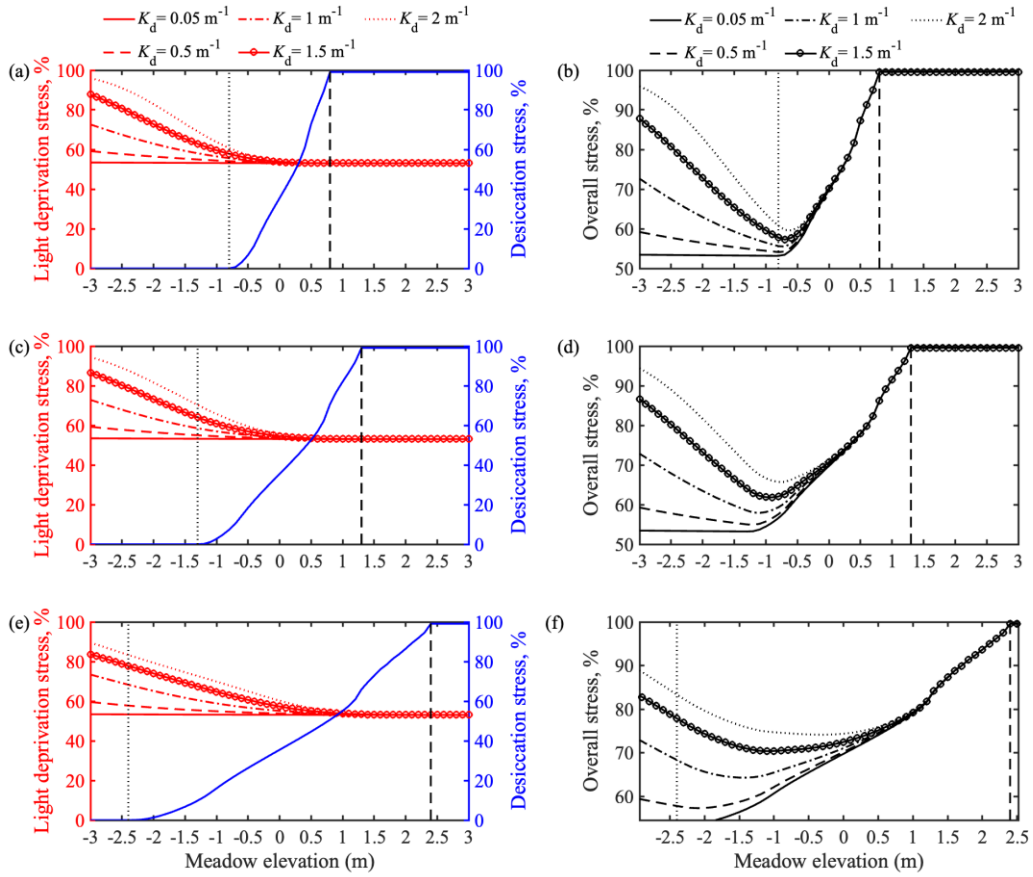

Figure 7 The modelled results of light deprivation stress and desiccation stress on 15 d-averaged seagrass growth with multiplicative formulation along the vertical depth gradient under different water turbidity conditions and tidal conditions. The separate effects of light deprivation stress and desiccation stress are shown in panels (a, c, e) and the combined effect of both stressors is shown in panels (b, d, f). Predictions are shown for microtidal conditions (a, b), mesotidal conditions (c, d), and macrotidal conditions (e, f). In each of the six panels, the black dotted line is the boundary between subtidal and lower intertidal zones, while the black dashed line is the boundary between upper intertidal and supratidal zones. The intertidal zone extends from -0.8 m to 0.8 m, -1.3 m to 1.3 m, and -2.4 m to 2.4 m for micro-, meso- and macro-tidal areas, respectively; The subtidal zone extends below -0.8 m, -1.3 m, and -2.4 m for micro-, meso- and macro-tidal areas, respectively; The supratidal zone extends above 0.8 m, 1.3 m, and 2.4 m for micro-, meso- and macro-tidal areas, respectively. Meadow elevation Z_b(m) is relative to mean sea level, and K_d (m^{-1}) is the light attenuation coefficient of the water column. These plots were constructed using the Baseline and Groups II, III and IV modelingscenarios (Supporting Information Table S3) that assumed the multiplicative formulation for $\mu(I, \mathrm{RWC})$.

In addition, the overall stress on intertidal seagrass growth, resulting from the cumulative effects of light deprivation and desiccation, was simulated using the reduction in seagrass growth rate from its potential maximum value, i.e., (1-$\mu/\mu_{\max}$) as a metric representing this overall stress (Figure 7b, d & f). The results indicate the presence of an "optimal" elevation for intertidal seagrasses where the cumulative stress arising from desiccation and light deprivation is minimized (e.g., at a meadow elevation approximately 0.5 m below mean sea level for seagrasses growing in microtidal conditions with water turbidity of K_d = 2 m^{-1} as shown in Figure 7b). At meadow elevations below the predicted optimal elevation, the overall stress increases with turbidity. This suggests that below the optimal elevation, the growth of intertidal seagrasses is primarily limited by light availability, and air exposure acts as the 'window' of photosynthetic relief from high turbidity to mediate the light deprivation stress. As elevation of the seagrass increases above the optimal elevation, the difference in overall stress between the different turbidity scenarios gradually diminishes. Thus, for seagrasses growing at elevations above the optimal elevation, desiccation becomes the dominant limiting factor for growth, and the negative effects of air exposure increasingly outweigh the positive effects of increased light moving further upward. Across all model scenarios we tested, the predicted optimal elevation shifts to lower elevations (more specifically, towards the lower intertidal zones), as turbidity reduces, although the curves tend to flatten. Note also that using the law of the minimum formulation does not change the conclusion (Supporting Information Figure S12).

The results confirm that light is a primary control of intertidal seagrass growth in the subtidal zones, while desiccation is a primary control in the supratidal zones. Our findings clearly suggest a trade-off between light deprivation and desiccation in relation to intertidal seagrass growth along the intertidal gradient, with an optimal elevation for seagrasses situated within the intertidal zone that maximises the benefits of light availability whilst minimising the detrimental effects of desiccation (Figure 7b, d & f).

4 Discussion

4.1 Species-specific physiological responses of intertidal seagrasses when air-exposed

Previous experimental studies have demonstrated the significance of physiological processes such as RWC loss and associated photosynthesis decline of different intertidal seagrass species when subject to air exposure (Jiang et al., 2014; Shafer et al., 2007). However, it is still uncertain how these physiological processes further limit the growth rate of intertidal seagrasses under different environmental conditions such as tidal range, meadow elevation and water turbidity. Our study introduced new data-calibrated formulations for intertidal seagrasses that quantify the decline of photosynthetic efficiency due to the changes of RWC when air-exposed. To do this, a comprehensive review of the literature on seagrass desiccation (Table 1) and the effects of this desiccation on photosynthetic efficiency (Supporting Information Figures S5-S7) was conducted. We then undertook targeted model simulations which demonstrated that air-exposed physiological processes (light- and RWC-dependent growth) can be substantially lower than if the air-exposed responses are neglected (light-dependent growth) (dashed lines in Figure 4). This suggests that neglecting the physiological response to air exposure can yield overestimation of growth rates for intertidal seagrasses.

We also examined the species-specific effect of desiccation on the growth rate of intertidal seagrasses by comparing the growth rate predictions made using three different $f_{\mathrm{RWC}}(\mathrm{RWC})$ functions (Eq. (9)-(11)) characterizing the changes of photosynthetic efficiency with the temporal decline of RWC due to short-term air exposure. These three $f_{\mathrm{RWC}}(\mathrm{RWC})$ functions are data-calibrated functions that we collate, justify and introduce in the present work. Our results suggest that the choice of the function $f_{\mathrm{RWC}}(\mathrm{RWC})$ characterizing the desiccation tolerance of different species substantially affects quantitative predictions of the physiological responses of intertidal seagrasses when air-exposed; if these functions are indeed species-specific, they may also suggest which species are more or less tolerant to desiccation. For example, desiccation-sensitive seagrass species such as temperate *H. johnsonii* and *C. nodosa* (Kahn & Durako, 2009; Papathanasiou et al., 2020) as well as temperate *N. japonica* and *Z. marina* (Shafer et al., 2007), whose response in photosynthetic efficiency is more likely to follow a linear (Eq. (9)) or sigmoidal curve (Eq. (11)) in relation to RWC loss, would experience an immediate and rapid decrease in growth rate following air exposure (red and blue lines in Supporting Information Figure S11). In contrast, desiccation-tolerant species such as tropical *T. hemprichii* and *E.*

acoroides (Jiang et al., 2014), whose response in photosynthetic efficiency is more likely to follow a hyperbolic tangent (Eq. (10)) in relation to RWC loss, may tolerate hours of air exposure without affecting their growth (green lines in Supporting Information Figure S11). However, we could only find data for six species to parameterise these $f_{\mathrm{RWC}}(\mathrm{RWC})$ functions. In the future, more species-specific studies can be incorporated; for example Bjork et al. (1999) reported that tropical intertidal seagrass species were more desiccation-resistant and were likely to have higher tolerances to thrive in the intertidal zones.

4.2 Trade-off between light deprivation and desiccation related to intertidal seagrass distribution

Along the intertidal gradient, both light availability and stress of desiccation gradually increase as meadow elevation increases. Light is a primary control on seagrass growth in subtidal zones, while desiccation is a primary control on seagrass growth in supratidal zones. However, in the intertidal zones, we observed in our simulations a clear trade-off between light deprivation and desiccation along the intertidal gradient (Figure 7), as a balance between obtaining enough light for their growth, while also avoiding the detrimental consequences of desiccation stress is vital for intertidal seagrasses. This is thus an "optimal" elevation for intertidal seagrasses which represents the minimized combined stress of light deprivation and desiccation. The location of this optimal elevation for intertidal seagrasses varies under different environmental conditions, such as tidal range and water turbidity. In all our model scenarios, the predicted optimal elevation occurs in the lower or intermediate intertidal zones. As water turbidity increases, the optimal elevation shifts upwards to higher elevations. The evaluation of optimal elevation has the potential to inform the most suitable habitat for intertidal seagrass growth.

Previous studies have found that differences in desiccation tolerances can be responsible for the seagrass distribution along the intertidal gradient. For example, in the intertidal seagrass meadows at the coasts of the Indo-Pacific, the desiccation-tolerant species *T. hemprichii* was found to be dominant in the upper intertidal zone while desiccation-sensitive species *H. uninervis* occupied the lower intertidal zone (Lan et al., 2005). However, increasing evidence suggests that photosynthetic responses to desiccation are insufficient to explain observed patterns of intertidal zonation (Shafer et al., 2007). Therefore, it is necessary to consider additional mechanisms, such as the combined effect of desiccation and light deprivation considered here, to explain the

observed zonation patterns of intertidal seagrasses. The trade-off between light deprivation and desiccation on intertidal seagrass distribution also finds some agreement with field studies demonstrating the intertidal zonation of different seagrass species. Huong et al. (2003) found that intertidal *N. japonica* in northern Vietnam occupied the intermediate intertidal zone while *H. ovalis* dominated in the lower intertidal zone, due to the different tolerances to low light availability (less in *N. japonica*) and desiccation (less in *H. ovalis*). Meanwhile, the seagrass *N. japonica* was also found to have the highest biomass in the intermediate intertidal zone on the southern coast of South Korea, where air exposure and light availability determined the upper and lower distributional limits, respectively (Kim et al., 2016). However, other environmental factors may also play an important role in defining the zonation of seagrass colonisation; Infantes et al. (2009) suggests that subtidal seagrasses have an upper depth limit controlled by shallow-water wave action, but the relevance of this limit to intertidal seagrasses may depend on the harshness of the local hydrodynamic conditions. Notably, intertidal seagrasses also evolve adaptation mechanisms to air exposure stress through adjustments to physiological characteristics followed by changes to morphology (Manassa et al., 2017; Park et al., 2016). For example, the enhanced photosynthetic performance after air exposure and the layout of the densely overlapped leaves to attain water are attributed as the adaptation mechanisms for *N. japonica* in the intertidal zone (Kim et al., 2020). Regardless of these complexities, understanding the trade-offs between stressors influencing the lower and upper meadow elevations of seagrasses is crucial for the effective management of these habitats, especially since intertidal zones are dynamic and challenging environments.

4.3 Model applications and future work

Our study emphasizes the importance of understanding the air-exposed physiological responses on the growth dynamics of intertidal seagrasses, and the growth rate functions we introduce can be immediately incorporated into a wide variety of process-based seagrass growth models. Although we are here only considering the impact of light and RWC on seagrass growth, the future application of the model components we introduce could also incorporate other interacting factors (e.g., temperature, nutrients) by the inclusion of appropriately defined additional functions (Baird et al., 2016; Elkalay et al., 2003; Turschwell et al., 2022). Our study provides conceptual and mathematical guidance for ecological modellers to include air-exposed responses

of intertidal seagrasses in their coastal ecosystem models. One example future application of our intertidal seagrass growth dynamics, of substantial interest, could be to simulate scenarios that assist in the selection of suitable sites for seagrass transplanting. Additionally, in recent years, global sea level rise and an increase in the input of terrestrial sediments pose a hazard to intertidal seagrass ecosystems (Flowers et al., 2023). These stressors simultaneously change the tidal regime and water turbidity, which affects the duration of air exposure/inundation periods and light availability. The model formulations we discuss in the present work can account for these cumulative stressors.

The comparisons between our data-calibrated model results and additional experimental studies also demonstrated the variability of physiological responses of intertidal seagrasses to air exposure, and hence the difficulty in transferring a model parameterised at one location/for one seagrass tissue to another location/tissue (Figure 3). This suggests that future experimental studies on the relationship between photosynthetic efficiency and air-exposure duration may therefore need to be species- or location-specific, to improve model predictions, although we recognise that this may often be prohibitively difficult or expansive to implement.

Additional environmental factors, such as wind and humidity, also play significant role in the desiccation of intertidal seagrass (Azevedo et al., 2017; Suykerbuyk et al., 2018), so are worthy of consideration in future modelling studies. Future modeling studies for intertidal seagrasses could also further incorporate delayed recovery processes of photosynthetic efficiency after re-submersion. Recovery of photosynthetic efficiency after re-submersion is critical for the seagrass growth response to desiccation stress (Park et al., 2016; Seddon & Cheshire, 2001; Shafer et al., 2007). When intertidal seagrasses are exposed to air for a prolonged duration, their photosynthetic efficiency may not be able to recover to their initial level after re-submersion. In the worst-case scenario, seagrasses may even lose the ability to resume photosynthesis (Shafer et al., 2007). There is not yet sufficient quantitative information available in the literature for us to confidently propose models of recovery of photosynthetic efficiency after re-submersion; this is an open question for future experimental research.

5 Conclusion

Through a comprehensive review of seagrass desiccation literature and the subsequent development of the first (to our knowledge) formulation of seagrass growth responses to air exposure, our study was able to explore how seagrass growth dynamics is affected by periodic tidal inundation and exposure under a wide range of environmental scenarios (tidal range, meadow elevation and water turbidity). We showed that neglecting physiological responses to air exposure for intertidal seagrasses results in overestimated growth rates, and we revealed a trade-off between light deprivation and desiccation on seagrass growth along intertidal gradients. More specifically, there is an "optimal" elevation for seagrasses where the combined stressors of desiccation and light deprivation are minimized, although the precise location of this optimal elevation will be highly system-specific. This finding may have future application in evaluating the viability of intertidal seagrass habitats and in informing decisions on coastal ecosystem management strategies such as nature-based solutions (e.g., living shorelines) under changing environmental conditions.. Overall, our work highlights the importance of elucidating the physiological responses of intertidal seagrasses in a highly dynamic and harsh environment and prompts further experimental studies to inform improved modeling of intertidal seagrass growth.

Acknowledgments

This work was supported by the National Key R&D Program of China (2019YFE0121500), the Australian Research Council (ARC) Discovery Early Career Researcher Award DE200100683, and the Scholarship from China Scholarship Council. The authors thank Severine Choukroun, Catherine Collier and Lucas Langlois for helpful discussions during manuscript development.

Data Availability Statement

Model code used in these simulations are available are available at Zenodo via https://doi.org/10.5281/zenodo.10466487.

References

Adams, J., and Bate, G. (1994), The tolerance to desiccation of the submerged macrophytes *Ruppia cirrhosa* (*Petagna*) *Grande* and *Zostera capensis Setchell*. *Journal of Experimental Marine Biology and Ecology. 183*(1), 53-62. https://doi.org/10.1016/0022-0981(94)90156-2

Adams, M. P. et al. (2020), Predicting seagrass decline due to cumulative stressors. *Environmental Modelling & Software. 130*, 104717. https://doi.org/10.1016/j.envsoft.2020.104717

Azevedo, A., Lillebø, A. I., Lencart e Silva, J., and Dias, J. M. (2017), Intertidal seagrass models: Insights towards the development and implementation of a desiccation module. *Ecological Modelling. 354*, 20-25. https://doi.org/10.1016/j.ecolmodel.2017.03.004

Baird, M. E. et al. (2016), A biophysical representation of seagrass growth for application in a complex shallow-water biogeochemical model. *Ecological Modelling. 325*, 13-27. https://doi.org/10.1016/j.ecolmodel.2015.12.011

Balke, T., Stock, M., Jensen, K., Bouma, T. J., and Kleyer, M. (2016), A global analysis of the seaward salt marsh extent: The importance of tidal range. *Water Resources Research. 52*(5), 3775-3786. https://doi.org/10.1002/2015wr018318

Bertelli, C. M., and Unsworth, R. K. F. (2018), Light Stress Responses by the Eelgrass, *Zostera marina (L)*. *Frontiers in Environmental Science. 6*, 39. https://doi.org/10.3389/fenvs.2018.00039

Bjork, M., Uku, J., Weil, A., and Beer, S. (1999), Photosynthetic tolerances to desiccation of tropical intertidal seagrasses. *Marine Ecology Progress Series. 191*, 121-126. https://doi.org/10.3354/meps191121

Cabaço, S., Machás, R., and Santos, R. (2009), Individual and population plasticity of the seagrass *Zostera noltii* along a vertical intertidal gradient. *Estuarine, Coastal and Shelf Science. 82*(2), 301-308. https://doi.org/10.1016j.ecss.2009.01.020

Carr, J. A., D'Odorico, P., McGlathery, K. J., and Wiberg, P. L. (2012), Stability and resilience of seagrass meadows to seasonal and interannual dynamics and environmental stress. *Journal of Geophysical Research: Biogeosciences. 117*(G1), 1007. https://doi.org/10.1029/2011JG001744

Che, X., Li, H., Zhang, L., and Liu, J. (2022), Effect of high light and desiccation on photosystem II in the seedlings and mature plants of tropical seagrass *Enhalus acoroides* during low tide. *Journal of Oceanology and Limnology. 41*, 241-250. https://doi.org/10.1007s00343-021-1170-2

Christensen, P., Díaz Almela, E., and Diekmann, O. 2004. Can transplanting accelerate the recovery of seagrasse? J. Borum, C. Duarte, D. Krause-Jensen, T.M. Greve (Eds.), European Seagrasses: an Introduction to Monitoring and Management, M&MS Project, Copenhagen, pp. 77-82

Clavier, J. et al. (2011), Aerial and underwater carbon metabolism of a *Zostera noltii* seagrass bed in the Banc d'Arguin, Mauritania. *Aquatic Botany. 95*(1), 24-30. https://doi.org/10.1016/j.aquabot.2011.03.005

Colomer, J., and Serra, T. (2021), The World of Edges in Submerged Vegetated Marine Canopies: From Patch to Canopy Scale. *Water. 13*(17), 2430. https://doi.org/10.3390/w13172430

de los Santos, C. B. et al. (2022), Sedimentary Organic Carbon and Nitrogen Sequestration Across a Vertical Gradient on a Temperate Wetland Seascape Including Salt Marshes, Seagrass Meadows and Rhizophytic Macroalgae Beds. *Ecosystems. 26*, 826–842. https://doi.org/10.1007/s10021-022-00801-5

Elkalay, K., Frangoulis, C., Skliris, N., Goffart, A., Gobert, S., Lepoint, G., and Hecq, J.-H. (2003), A model of the seasonal dynamics of biomass and production of the seagrass *Posidonia oceanica* in the Bay of Calvi (Northwestern Mediterranean). *Ecological Modelling. 167*(1-2), 1-18. https://doi.org/10.1016S0304-3800(03)00074-7

Erftemeijer, P. L. A., van Gils, J., Fernandes, M. B., Daly, R., van der Heijden, L., and Herman, P. M. J. (2023), Habitat suitability modelling to improve understanding of seagrass loss and recovery and to guide decisions in relation to coastal discharge. *Marine pollution bulletin. 186*, 114370. https://doi.org/10.1016/j.marpolbul.2022.114370

Espadero, A. D. A., Nakamura, Y., Uy, W. H., Tongnunui, P., and Horinouchi, M. (2020), Tropical intertidal seagrass beds: An overlooked foraging habitat for fishes revealed by underwater videos. *Journal of Experimental Marine Biology and Ecology. 526*, 151353. https://doi.org/10.1016/j.jembe.2020.151353

Fan, Y., Chen, S., Pan, S., and Dou, S. (2020), Storm-induced hydrodynamic changes and seabed erosion in the littoral area of Yellow River Delta: A model-guided mechanism study. *Continental Shelf Research. 205*. https://doi.org/10.1016/j.csr.2020.104171

Flowers, G. J. L., Needham, H. R., Bulmer, R. H., Lohrer, A. M., and Pilditch, C. A. (2023), Going under: The implications of sea-level rise and reduced light availability on intertidal primary production. *Limnology and Oceanography. 68*, 1301-1315. https://doi.org/10.1002/lno.12347

961 Folmer, E. O., van der Geest, M., Jansen, E., Olff, H., Michael Anderson, T., Piersma, T., and van Gils, J. A. (2012),
962 Seagrass–Sediment Feedback: An Exploration Using a Non-recursive Structural Equation Model.
963 *Ecosystems. 15*(8), 1380-1393. https://doi.org/10.1007/s10021-012-9591-6
964 Geary, W. L. et al. (2020), A guide to ecosystem models and their environmental applications. *Nature ecology &*
965 *evolution. 4*(11), 1459-1471. https://doi.org/10.1038/s41559-020-01298-8
966 Huong, T. T. L., Vermaat, J. E., Terrados, J., Van Tien, N., Duarte, C. M., Borum, J., and Tri, N. H. (2003),
967 Seasonality and depth zonation of intertidal *Halophila ovalis* and *Zostera japonica* in Ha Long Bay
968 (northern Vietnam). *Aquatic Botany. 75*(2), 147-157. https://doi.org/10.1016S0304-3770(02)00172-9
969 Infantes, E., Terrados, J., Orfila, A., Cañellas, B., and Álvarez-Ellacuria, A. (2009), Wave energy and the upper
970 depth limit distribution of *Posidonia oceanica*. *Botanica Marina. 52*(5), 419-427.
971 https://doi.org/10.1515/BOT.2009.050
972 Jarvis, J. C., Brush, M. J., and Moore, K. A. (2014), Modeling loss and recovery of *Zostera marina* beds in the
973 Chesapeake Bay: The role of seedlings and seed-bank viability. *Aquatic Botany. 113*, 32-45.
974 https://doi.org/10.1016j.aquabot.2013.10.010
975 Jassby, A. D., and Platt, T. (1976), Mathematical formulation of the relationship between photosynthesis and light
976 for phytoplankton. *Limnology and Oceanography. 21*(4), 540-547.
977 https://doi.org/10.4319/lo.1976.21.4.0540
978 Jiang, Z., Huang, X., Zhang, J., Zhou, C., Lian, Z., and Ni, Z. (2014), The effects of air exposure on the desiccation
979 rate and photosynthetic activity of *Thalassia hemprichii* and *Enhalus acoroides*. *Marine Biology. 161*(5),
980 1051-1061. https://doi.org/10.1007/s00227-014-2398-6
981 Johnson, I. R., and Thornley, J. H. M. (1984), A model of instantaneous and daily canopy photosynthesis. *Journal of*
982 *Theoretical Biology. 107*(4), 531-545. https://doi.org/10.1016/S0022-5193(84)80131-9
983 Kahn, A. E., and Durako, M. J. (2009), Photosynthetic tolerances to desiccation of the co-occurring seagrasses
984 *Halophila johnsonii* and *Halophila decipiens*. *Aquatic Botany. 90*(2), 195-198.
985 https://doi.org/10.1016/j.aquabot.2008.07.003
986 Kaldy, J. (2012), Influence of light, temperature and salinity on dissolved organic carbon exudation rates in *Zostera*
987 *marina L*. *Aquatic Biosystems. 8*(1), 19. https://doi.org/10.1186/2046-9063-8-19
988 Kim, J.-H., Kim, S. H., Kim, Y. K., Park, J.-I., and Lee, K.-S. (2016), Growth dynamics of the seagrass *Zostera*
989 *japonica* at its upper and lower distributional limits in the intertidal zone. *Estuarine, Coastal and Shelf*
990 *Science. 175*, 1-9. https://doi.org/10.1016/j.ecss.2016.03.023
991 Kim, S. H., Kim, J. W., Kim, Y. K., Park, S. R., and Lee, K. S. (2020), Factors controlling the vertical zonation of
992 the intertidal seagrass, *Zostera japonica* in its native range in the northwestern Pacific. *Marine*
993 *Environmental Research. 157*, 104959. https://doi.org/10.1016/j.marenvres.2020.104959
994 Kirk, J. T. (1985), Effects of suspensoids (turbidity) on penetration of solar radiation in aquatic ecosystems.
995 *Hydrobiologia. 125*, 195-208. https://doi.org/10.1007/BF00045935
996 Koch, E. W. (2001), Beyond light: physical, geological, and geochemical parameters as possible submersed aquatic
997 vegetation habitat requirements. *Estuaries. 24*, 1-17. https://doi.org/10.2307/1352808
998 Lan, C.-Y., Kao, W.-Y., Lin, H.-J., and Shao, K.-T. (2005), Measurement of chlorophyll fluorescence reveals
999 mechanisms for habitat niche separation of the intertidal seagrasses *Thalassia hemprichii* and *Halodule*
1000 *uninervis*. *Marine Biology. 148*(1), 25-34. https://doi.org/10.1007/s00227-005-0053-y
1001 Leuschner, C., Landwehr, S., and Mehlig, U. (1998), Limitation of carbon assimilation of intertidal *Zostera noltii*
1002 and *Z. marina* by desiccation at low tide. *Aquatic Botany. 62*(3), 171-176. https://doi.org/10.1016S0304-
1003 3770(98)00091-6
1004 Manassa, R. P., Smith, T. M., Beardall, J., Keough, M. J., and Cook, P. L. M. (2017), Capacity of a temperate
1005 intertidal seagrass species to tolerate changing environmental conditions: Significance of light and tidal
1006 exposure. *Ecological Indicators. 81*, 578-586. https://doi.org/10.1016/j.ecolind.2017.04.056
1007 Moreno-Marín, F., Brun, F. G., and Pedersen, M. F. (2018), Additive response to multiple environmental stressors in
1008 the seagrass *Zostera marina L*. *Limnology and Oceanography. 63*(4), 1528-1544.
1009 https://doi.org/10.1002/lno.10789
1010 Olesen, B., and Sand-Jensen, K. (1993), Seasonal acclimatization of eelgrass *Zostera marina* growth to light.
1011 *Marine Ecology Progress Series. 94*, 91-91. https://doi.org/10.3354/meps094091
1012 Orth, R. J. et al. (2020), Restoration of seagrass habitat leads to rapid recovery of coastal ecosystem services.
1013 *Science Advances. 6*(41), eabc6434. https://doi.org/10.1126/sciadv.abc6434
1014 Papathanasiou, V., Kariofillidou, G., Malea, P., and Orfanidis, S. (2020), Effects of air exposure on desiccation and
1015 photosynthetic performance of *Cymodocea nodosa* with and without epiphytes and *Ulva rigida* in
1016 comparison, under laboratory conditions. *Marine Environmental Research. 158*, 104948.

https://doi.org/10.1016/j.marenvres.2020.104948
Park, S. R., Kim, S., Kim, Y. K., Kang, C. K., and Lee, K. S. (2016), Photoacclimatory Responses of *Zostera marina* in the Intertidal and Subtidal Zones. *PLoS One. 11*(5), e0156214. https://doi.org/10.1371/journal.pone.0156214
Park, S. R., Moon, K., Kim, S. H., and Lee, K.-S. (2021), Growth and Photoacclimation Strategies of Three *Zostera* Species Along a Vertical Gradient: Implications for Seagrass Zonation Patterns. *Frontiers in Marine Science. 8*, 594779. https://doi.org/10.3389/fmars.2021.594779
Pérez-Lloréns, J., Strother, S., and Niell, F. (1994), Species differences in short-term pigment levels in four Australian seagrasses in response to desiccation and rehydration. *Botanica Marina. 37*, 91-96. https://doi.org/10.1515botm.1994.37.1.91
Petrou, K., Jimenez-Denness, I., Chartrand, K., McCormack, C., Rasheed, M., and Ralph, P. J. (2013), Seasonal heterogeneity in the photophysiological response to air exposure in two tropical intertidal seagrass species. *Marine Ecology Progress Series. 482*, 93-106. https://doi.org/10.3354/meps10229
Piercy, C. D., Charbonneau, B. R., Russ, E. R., and Swannack, T. M. (2023), Examining the commonalities and knowledge gaps in coastal zone vegetation simulation models. *Earth Surface Processes and Landforms.* 1-25. https://doi.org/10.1002/esp.5565
Poorter, H., Anten, N. P., and Marcelis, L. F. (2013), Physiological mechanisms in plant growth models: do we need a supra-cellular systems biology approach? *Plant Cell & Environment. 36*(9), 1673-1690. https://doi.org/10.1111/pce.12123
Scalpone, C. R., Jarvis, J. C., Vasslides, J. M., Testa, J. M., and Ganju, N. K. (2020), Simulated Estuary-Wide Response of Seagrass (*Zostera marina*) to Future Scenarios of Temperature and Sea Level. *Frontiers in Marine Science. 7*, 873. https://doi.org/10.3389/fmars.2020.539946
Seddon, S., and Cheshire, A. C. (2001), Photosynthetic response of *Amphibolis antarctica* and *Posidonia australis* to temperature and desiccation using chlorophyll fluorescence. *Marine Ecology Progress Series. 220*, 119-130. https://doi.org/10.3354/meps220119
Shafer, D. J., Sherman, T. D., and Wyllie-Echeverria, S. (2007), Do desiccation tolerances control the vertical distribution of intertidal seagrasses? *Aquatic Botany. 87*(2), 161-166. https://doi.org/10.1016/j.aquabot.2007.04.003
Silva, J., Santos, R., Calleja, M. L., and Duarte, C. M. (2005), Submerged versus air-exposed intertidal macrophyte productivity: from physiological to community-level assessments. *Journal of Experimental Marine Biology and Ecology. 317*(1), 87-95. https://doi.org/10.1016/j.jembe.2004.11.010
Simpson, M. J., Browning, A. P., Warne, D. J., Maclaren, O. J., and Baker, R. E. (2022), Parameter identifiability and model selection for sigmoid population growth models. *Journal of Theoretical Biology. 535*, 110998. https://doi.org/10.1016/j.jtbi.2021.110998
Suykerbuyk, W. et al. (2018), Living in the intertidal: desiccation and shading reduce seagrass growth, but high salinity or population of origin have no additional effect. *PeerJ. 6*, e5234. https://doi.org/10.7717/peerj.5234
Tanaka, Y., and Nakaoka, M. (2004), Emergence stress and morphological constraints affect the species distribution and growth of subtropical intertidal seagrasses. *Marine Ecology Progress Series. 284*, 117-131. https://doi.org/10.3354/meps284117
Tian, R. C. (2006), Toward standard parameterizations in marine biological modeling. *Ecological Modelling. 193*(3-4), 363-386. https://doi.org/10.1016/j.ecolmodel.2005.09.003
Toublanc, F., Brenon, I., Coulombier, T., and Le Moine, O. (2015), Fortnightly tidal asymmetry inversions and perspectives on sediment dynamics in a macrotidal estuary (Charente, France). *Continental Shelf Research. 94*, 42-54. https://doi.org/10.1016/j.csr.2014.12.009
Turschwell, M. P. et al. (2022), Interactive effects of multiple stressors vary with consumer interactions, stressor dynamics and magnitude. *Ecology Letters. 25*(6), 1483-1496. https://doi.org/10.1111/ele.14013
Vieira, V. M. N. C. S., Lopes, I. E., and Creed, J. C. (2018), The biomass–density relationship in seagrasses and its use as an ecological indicator. *BMC Ecology. 18*(1), 44. https://doi.org/10.1186/s12898-018-0200-1
Wang, X. (2024), ceeh-bnu/Intertidal-seagrass: Intertidal seagrass model (Version V4) [Software]. Zenodo. https://doi.org/10.5281/zenodo.10825317
Wang, X., Bai, J., Yan, J., Cui, B., and Shao, D. (2022), How Turbidity Mediates the Combined Effects of Nutrient Enrichment and Herbivory on Seagrass Ecosystems. *Frontiers in Marine Science. 9*, 787041. https://doi.org/10.3389/fmars.2022.787041
Wang, X., Yan, J., Bai, J., Shao, D., and Cui, B. (2021), Effects of interactions between macroalgae and seagrass on the distribution of macrobenthic invertebrate communities at the Yellow River Estuary, China. *Marine*

Pollution Bulletin. 164, 112057. https://doi.org/10.1016/j.marpolbul.2021.112057

Waycott, M. et al. (2009), Accelerating loss of seagrasses across the globe threatens coastal ecosystems. *Proceedings of the National Academy of Sciences. 106*(30), 12377-12381. https://doi.org/10.1073pnas.0905620106

Wuthirak, T., Kongnual, R., and Buapet, P. (2016), Desiccation tolerance and underlying mechanisms for the recovery of the photosynthetic efficiency in the tropical intertidal seagrasses *Halophila ovalis* and *Thalassia hemprichii*. *Botanica Marina. 59*(5), 387-396. https://doi.org/doi:10.1515/bot-2016-0052

Zhang, X. et al. (2019), A unique meadow of the marine angiosperm *Zostera japonica*, covering a large area in the turbid intertidal Yellow River Delta, China. *Science of The Total Environment. 686*, 118-130. https://doi.org/10.1016/j.scitotenv.2019.05.320

Zhou, Q., Ke, Y., Wang, X., Bai, J., Zhou, D., and Li, X. (2022), Developing seagrass index for long term monitoring of *Zostera japonica* seagrass bed: A case study in Yellow River Delta, China. *ISPRS Journal of Photogrammetry and Remote Sensing. 194*, 286-301. https://doi.org/10.1016/j.isprsjprs.2022.10.011